Bound, odd-parity $J = 1$ spectra of the alkaline earths: Ca, Sr, and Ba

J. A. Armstrong and J. J. Wynne
IBM Thomas J. Watson Research Center, P.O. Box 218 Yorktown Heights, New York 10598

P. Esherick
Sandia Laboratories, Division 5216, Albuquerque, New Mexico 87115
(Received 13 July 1978)

We have used multiphoton excitation *via* selected intermediate states to observe and identify triplet Rydberg series of the type $msnp\ ^3P^0$ up to high n in Ca, Sr, and Ba. Previous efforts have failed to identify these series beyond $n = 7$. We present details of our experimental method, give tables of the newly determined energy levels, and describe their analysis by multi-channel quantum defect theory (MQDT). For the most part, the $msnp\ ^3P^0$ series in Ca and Sr can be described by a nearly constant quantum defect δ with $\delta_{Ca} = 19.7$ and $\delta_{Sr} = 2.90$. The $6s\,np\ ^3P^0$ series in Ba is more heavily affected by the configuration interaction, but to a reasonable approximation has $\delta_{Ba} \approx 3.81$. For all three elements, we find that the $msnp\ ^1P_1^0$ series are much more strongly perturbed than the $^3P_1^0$ series. Most of this paper treats Ba. In addition to the $^3P^0$ states, $^3F_2$ and $^1G_4$ states are measured and tabulated. Further results in Ba include new and/or revised values for some $^1P_1^0$ states a revised ionization limit, evidence for an energy-dependent configuration interaction, and an MQDT prediction of the photoabsorption cross section at the ionization limit. This prediction agrees with the most recent experimental cross section. The MQDT analysis of Ba is described in great detail to make it useful as a guide to the reader who wishes to become a user of MQDT.

I. INTRODUCTION

Alkaline earth atoms have bound Rydberg series which may be classified by the approximate configurational labels *msnl* and which are primarily Russell-Saunders coupled, i.e., L and S are good quantum numbers. Although absorption spectra of these atoms have revealed extensive singlet series, the corresponding triplet series are largely unknown. The absorption spectra of Ca, Sr, and Ba ($m = 4$, 5, and 6 respectively) correspond to transitions from the even-parity $ms^2\ ^1S_0$ ground states to odd-parity, $J = 1$ states. From photographic absorption spectra, the singlet $msnp\ ^1P_1^0$ series have been observed up to $n_{Ca} = 79$,[1] $n_{Sr} = 60$,[2,3] and $n_{Ba} = 75$.[4] But the corresponding triplet $msnp\ ^3P_1^0$ levels have only been correctly identified in absorption to $n_{Ca} = 7$,[5] $n_{Sr} = 7$,[6] and $n_{Ba} = 7$.[7]

The principal $^1P_1^0$ series are known to be perturbed by states with the configurational labels $3d4p$ in Ca, $4d5p$ in Sr and $5d6p$, $5d7p$ and $5d8p$ in Ba. Furthermore, one perturber from $5d4f$ had also been identified in Ba.[4] Despite the small number of $msnp\ ^3P_1^0$ states seen in absorption, the triplet perturbers $3d4p\ ^3P_1^0$ and $^3D_1^0$ in Ca, $4d5p\ ^3P_1^0$ and $^3D_1^0$ in Sr, and $5d6p$, $5d7p$ and $5d8p\ ^3P_1^0$ and $^3D_1^0$ in Ba have also been identified.

We have used multiphoton excitation *via* selected intermediate states to overcome the spin-forbidden nature of transitions from the $ms^2\ ^1S_0$ ground state to the $msnp\ ^3P_1^0$ excited states and have observed triplet Rydberg series up to high n for Ca, Sr, and Ba. In this paper, we present details of our experimental method, give tables of the newly determined energy levels, and describe their analysis by multichannel quantum defect theory[8] (MQDT).

In an earlier paper,[9] we gave a preliminary report on Ca and Sr. These atoms have simpler triplet spectra than Ba because of the presence of only one important perturber, $3d4p\ ^3P_1^0$ and $4d5p\ ^3P_1^0$ for Ca and Sr, respectively. These perturbers lie relatively low in energy and perturb the Rydberg spectra only slightly. For most practical purposes, the $msnp\ ^3P_1^0$ Rydberg series of Ca and Sr can be described by constant quantum defect δ; $\delta_{Ca} = 1.97$ and $\delta_{Sr} = 2.90$. Our results for Ca and Sr include determination of a number of the $J = 0$ and 2, $^3P^0$ states, as well as the $J = 1$ states.

The major part of this paper deals with our work on the odd-parity, $J = 1$ spectrum of Ba. This spectrum is complicated by 12 perturbers, including one, the $5d8p\ ^1P_1^0$, which lies "astride" the $6s$ ionization limit and interacts with many, high-lying, bound members of the $6snp\ ^1P_1^0$ series. Experiment shows that the $6snp\ ^1P_1^0$ series is much more strongly perturbed than the $6snp\ ^3P_1^0$ series (which has $\delta_{Ba} \approx 3.81$). This is because the configuration interaction for singlets is much greater than for triplets. The fact that the $6snp\ ^1P_1^0$ series is clearly perturbed by $5dnp\ ^3D_1^0$ and $^3P_1^0$, as well as by $^1P_1^0$, reflects the importance of spin-orbit coupling in the $5dnp$ channels. That is, the perturbers are far from being L-S coupled in barium.

This paper is organized as follows: Section II describes our experimental technique; Sec. III presents our values for the newly identified energy levels; Sec. IV describes our analysis of the Rydberg series and their interactions by MQDT; and Sec. V is a discussion. Among the important results described for Ba are: (*i*) new $^3P_1^0$ term values; (*ii*) new and/or revised values for some $^1P_1^0$ states; (*iii*) MQDT analysis of all $J = 1$ states; (*iv*) evidence for an energy-dependent configuration interaction; and (*v*) an accurate MQDT prediction of the photoabsorption cross section at the ionization limit.

II. EXPERIMENTAL TECHNIQUES

Multiphoton ionization spectroscopy[10] (MIS) permits observation of excited states which are not ordinarily observed in one photon excitation from the ground state. For example, term values for the $msnp\ ^3P_1^0$ states of Ca, Sr, and Ba for $n > 7$ have not so far been published.[11] We have used a three-laser technique to enter the triplet manifold and do excitation spectra of the $msnp\ ^3P^0$ states. The basic experimental

 0030-3941/79/020211-20$00.50

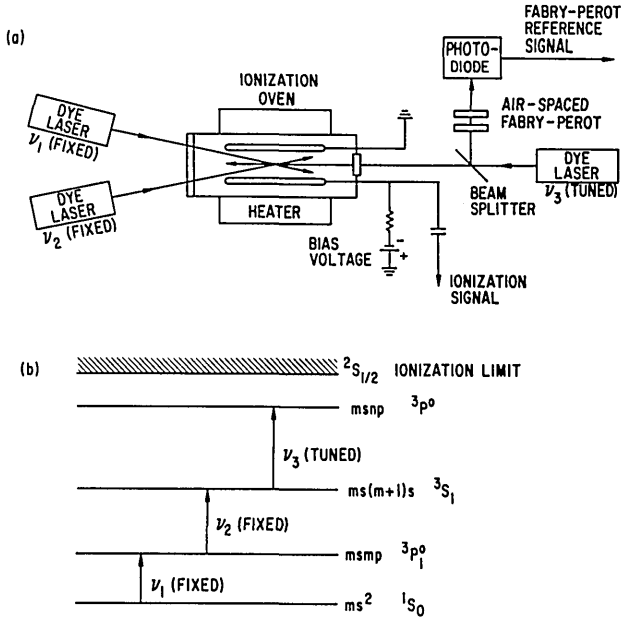

FIG. 1. (a) Experimental set-up for three-laser excitation of atomic vapors with ionization detection and reference signal for calibration. (b) Energy-level diagram of typical alkaline earth atom showing sequence which allows for easy excitation of $^3P^0$ states.

method is diagrammed in Fig. 1. A laser at frequency ν_1 excites atoms from the $(ms)^2\,{}^1S_0$ ground state to the $msmp\ {}^3P_1^0$ state. This so-called intercombination transition has an oscillator strength of $f \cong 5 \times 10^{-5}$, 10^{-3}, and 10^{-2} for Ca, Sr, and Ba, respectively. Although it is relatively forbidden [compared to the $(ms)^2\,{}^1S_0$-to-$msmp\ {}^1P_1^0$ transition with $f \cong 1.7$, 1.9, and 1.6 in Ca, Sr, and Ba], the transition may easily be saturated with intensities available from nitrogen-laser-pumped dye lasers. A second laser (ν_2) then excites atoms from the $msmp\ {}^3P_1^0$ state to the $ms(m+1)\ {}^3S_1$ state, the lowest $^3S_1$ state. This transition is strongly allowed ($f \sim 1$) and is easily saturated. To obtain a triplet spectrum, the ionization signal is monitored as a third laser (ν_3) is tuned through transitions from the populated $^3S_1$ level to high-energy $msnp\ {}^3P^0$ states, up to the $^2S_{1/2}$ ionization limit. The high-lying Rydberg states are probably ionized by a collisional mechanism.

The ionization detector works as a space-charge limited, thermionic diode and has substantial gain.[12] This detector was first studied by Kingdon[13] and has been referred to as the "Kingdon Cage." For these experiments, a pipe, having an inner diameter of ~3.5 cm and a heated region ~30 cm long, contained the atomic vapor. The pipe was, typically, heated to 700–800 °C, and produced vapor pressures of ~0.2–1.0 Torr in Ca, Sr, and Ba. The ionization-detecting electrodes were parallel plates with 30 cm × 1 cm faces, held ~0.5 cm apart with spacers. A −1 V bias was applied in series with a 500 KΩ load resistor. Pulsed voltage was then measured at the negative electrode through a coupling capacitor. More details on the detector may be found in Ref. 14. For Ca and Sr, the pipe was operated at temperatures for which the metals did not melt, and ~10-Torr Ne buffer gas was added to reduce the diffusion of metal vapor out of the heated zone of the pipe. Ba data was taken at temperatures above the Ba melting point at ~1-Torr Ba pressure. The three dye lasers, simple Hänsch-type oscillators,[15] were simultaneously pumped by split beams from a Molectron UV-1000 nitrogen laser. Each dye laser produced ~10 kW peak power in the form of ~10-ns-long pulses with ~0.2-cm^{-1} linewidth. The lasers were pulsed at 13 (⅓) pps, and the signal was averaged with a linear gate (see Ref. 14 for more details). The averaged output could be displayed on a strip chart recorder or fed into an IBM 370/168 computer *via* an IBM 7406 Device Coupler.

The laser beams overlapped at the center of the pipe, between the ionization-detecting electrodes. The specific arrangement of Fig. 1 is not essential but was chosen for convenience. All three beams could propagate collinearly if desired. The frequencies were set as follows: frequency ν_1 was set by blocking the other two lasers and tuning ν_1 until an ionization signal from the $msmp\ {}^3P_1^0$ state was seen. Light from the laser at ν_2 was then added and ν_2 tuned so that ν_1 and ν_2 combined produced a stronger ionization signal than ν_1 alone. These lasers were then attenuated to reduce the signal down to the noise level. Since the $^3P_1^0$-$^3S_1$ transition is strongly allowed and easily saturated, very strong attenuation ($\sim 10^3$) was needed for the beam at ν_2. The third laser was then added, and the ionization signal as a function of ν_3 was recorded.

A representative spectrum of Ca is shown in Fig. 2. Frequency markers at ~1-cm^{-1} intervals were recorded on each scan by monitoring the transmission of part of the ν_3 beam through an air-spaced Fabry-Perot interferometer (Fig. 1). The Fabry-Perot interferometer was constructed with fused quartz and a fused quartz spacer to minimize thermal drift. No systematic drift in the spacing due to thermal expansion or distortion was detectable.

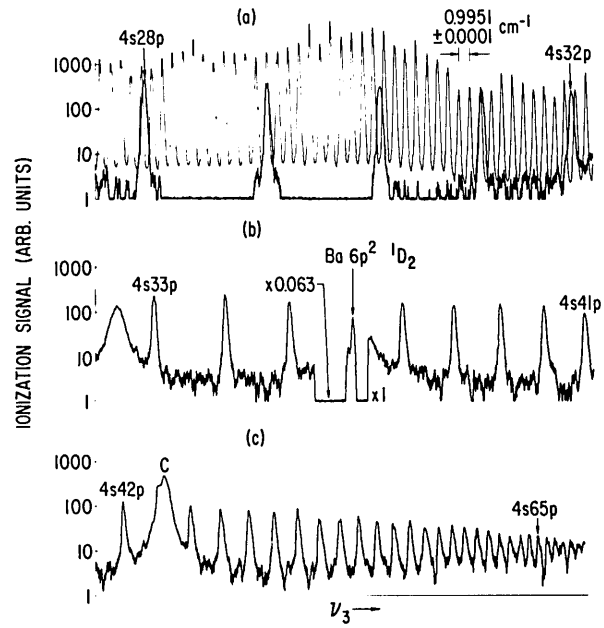

FIG. 2. Ionization signal in Ca as a function of ν_3. Scan (a) shows the Fabry-Perot reference signal used for calibration. Scan (b) has a change of scale around the state labelled Ba $6p^2\ {}^1D_2$. This state appears due to a two-photon transition ($2\nu_3$) in Ba impurity atoms. The Ca $4s36p\ {}^3P^0$ state appears as a low-energy, partially resolved shoulder on the Ba $6p^2\ {}^1D_2$ peak. Scan (c) shows a broad peak, labelled C, which is due to collisional population of a lower level, not intentionally excited, followed by a one-photon (ν_3) excitation.

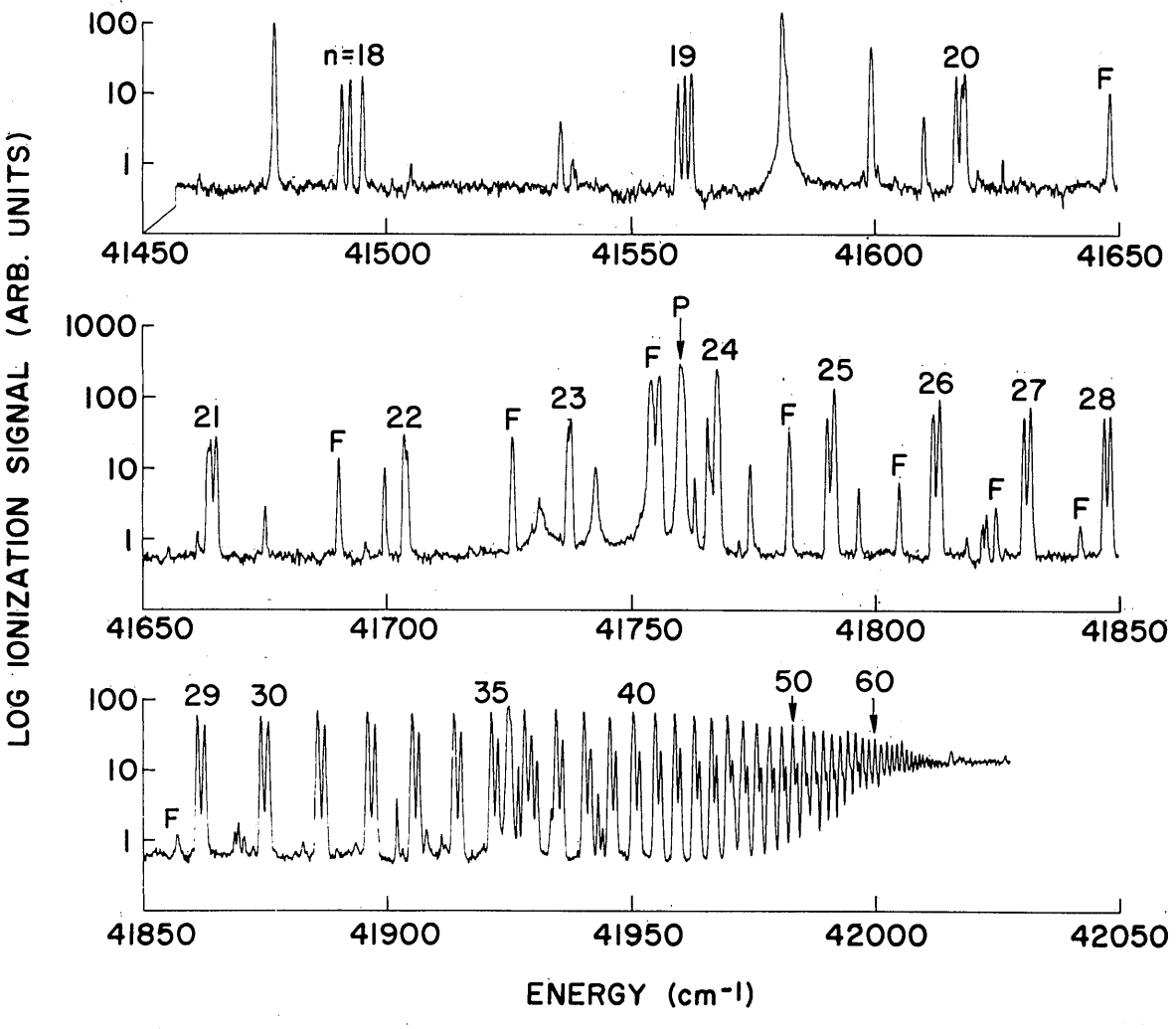

FIG. 3. Multiphoton ionization spectrum of Ba. The numerical labels correspond to the principal quantum number n ($6snp$) while the alphabetic labels designate F states and a perturber P (see text in Sec. IV E).

The Fabry-Perot fringes were calibrated by a least-squares fit, linear in frequency, to the position of ionization signal peaks due to known transitions. Then, unknown peaks in the ionization signal were measured against the calibrated fringes by interpolation between adjacent fringes. For data taken on the strip chart recorder, the measurement of peaks and interpolation was done by hand. This was the case for all of our data on Ca and Sr. The data analysis for Ba was considerably speeded and simplified by use of the computer. Here, with the aid of a graphic display terminal, peaks could be selected visually and then located and calibrated by computer.

The excitation sequence described above was sufficient for identifying $^3P^0$ states in Ca and Sr. Here transitions for the $ms(m+1)s\ ^3S_1$ state to the $msnp\ ^1P_1^0$ states were weak and, where observable, appeared as side peaks or shoulders on the main signal peaks due to the $ms(m+1)s\ ^3S_1$-to-$msnp\ ^3P^0$ transitions. Such additional peaks provided convenient calibration points, since the positions of the $msnp\ ^1P_1^0$ states are well known.[1,3] Additional calibration points were provided by known transitions in Ba and Na, which were present as impurities in Ca and Sr.

In contrast to Ca and Sr, a spectrum for Ba, such as that shown in Fig. 3, has several strong peaks for each value of the principal quantum number (n), and it is not at first clear how to identify them. From an independent calibration, using a ½-m Jarrell-Ash monochromator, some of the peaks were found to correspond to $6snp\ ^1P_1^0$ states, as measured by Garton and Tomkins.[4] These peaks are stronger than the others, especially as one approaches the ionization limit. The other peaks correspond to $6snp\ ^3P^0$ states, with $J = 0$, 1 and 2 all being accessible from $6s7s\ ^3S_1$. Furthermore, the region around $n = 23$ and 24 is confused by many peaks and by the fact that the $6s23p$ and $6s24p\ ^1P_1^0$ states had not been photographically observed in absorption[4] and therefore had not been previously identified. To help sort out this spectrum, we took our own absorption measurements, and we also used a complementary three-step excitation with the $6s7s\ ^1S_0$ as an intermediate state.

For the absorption studies, the second harmonic light from a single dye laser passed through two pipes, one containing Ba and the other containing Na. The transmission was monitored with a photomultiplier as the laser was scanned. Part of the laser was also sent through the Fabry-Perot interfer-

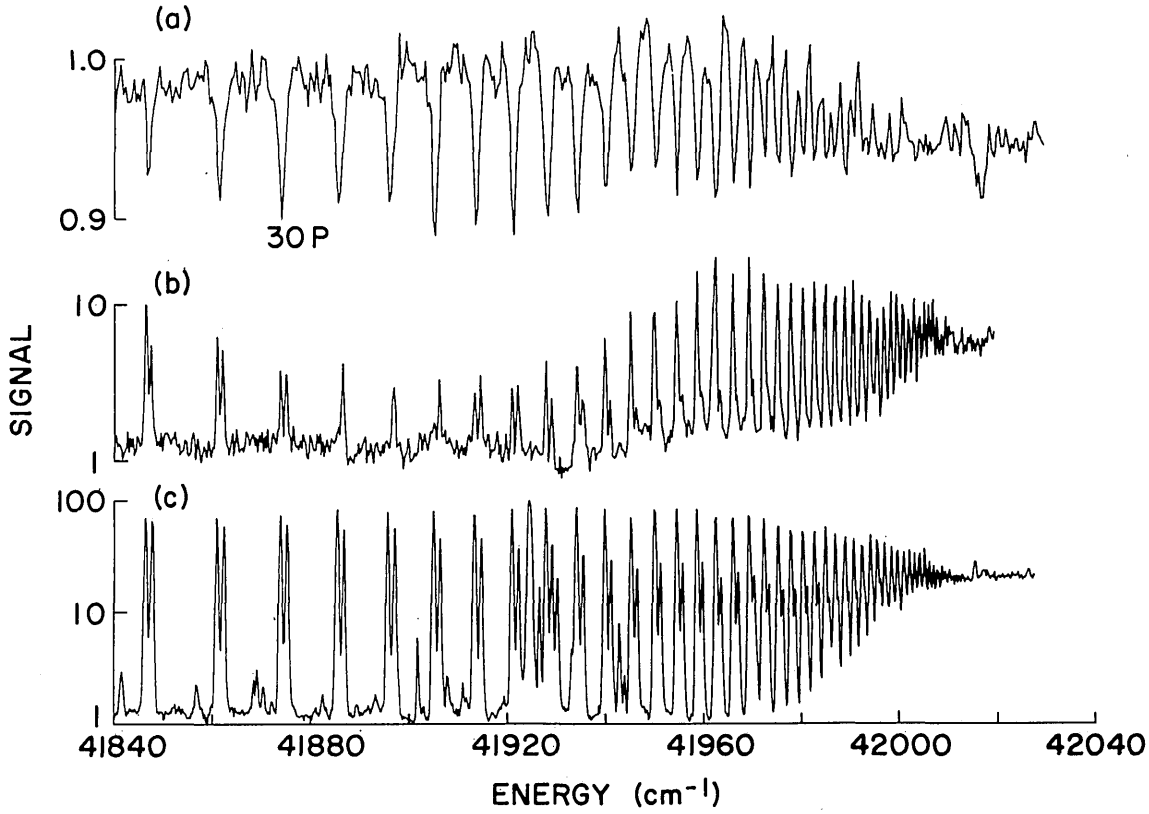

FIG. 4. Spectra of Ba taken by (a) one-photon absorption, (b) three-photon excitation and ionization *via* the $6s7s\ ^1S_0$, and (c) three-photon excitation and ionization *via* the $6s7s\ ^3S_1$. The vertical scale for (a) is linear and for (b) and (c) is logarithmic. The scans have been put on a common horizontal scale. Note that the states that appear in all three spectra at the same energy are $6snp\ ^1P_1^0$. The $6s30p$ state is marked.

ometer. The pipe containing Ba had a heated zone ~120-cm long and typically operated with a Ba vapor pressure of ~1 Torr. The pipe containing Na had a heated zone ~25-cm long and typically operated with a Na vapor pressure of ~2 Torr. The second harmonic light passed through both pipes in series. The laser was frequency doubled in non-phasematched KDP or ADP to avoid the problems of large variations in the second harmonic power as the frequency was scanned.[14] The Na absorption lines, corresponding to one-photon transitions from the 3*s* ground state to the *np* excited states, are well known and were used to calibrate the Fabry-Perot fringes from which the Ba absorption peaks were measured.

These absorption measurements confirmed the positions of the higher $6snp\ ^1P_1^0$ states as measured by Garton and Tomkins[4] and as observed in our three-laser experiment using the $6s7s\ ^3S_1$ state as an intermediate (Fig. 3). The $6s23p\ ^1P_1^0$ state was detectable in absorption as a weak peak, but the $6s24p\ ^1P_1^0$ was not. (However, see Ref. 11.) Furthermore, as will be seen below, we found values for some of the low-lying $6snp\ ^1P_1^0$ states which differ from the literature.[7]

To calibrate the three step excitation spectra, known values for several two-photon transitions in Ba, as well as for the $6snp\ ^1P_1^0$ states, were used. The $6snp\ ^1P_1^0$ state values for $n = 11$ and 12 were taken from our absorption measurements. Those for $n = 13$ and 14 were taken from Garton and Codling,[16] and those for $n \geq 15$ from Garton and Tomkins.[4]

Having identified the $^1P_1^0$ states in our spectra, we still had to positively identify the $^3P^0$ states seen in the three-step excitation. Excitation *via* the $6s7s\ ^1S_0$ state results in the excitation of $J = 1$ states only. Such spectra clearly show pairs of peaks (see Fig. 4), one set of which corresponds to the $6snp\ ^1P_1^0$ states. We identified the other set as the $6snp\ ^3P_1^0$ peaks. With this identification, we were able to identify the peaks in the excitation spectra seen from the $6s7s\ ^3S_1$ state. In addition to the $6snp\ ^1P_1^0$ and $^3P_1^0$ states, we observed a series of peaks we attributed to the $6snp\ ^3P_2^0$ states. These peaks were stronger than the $^3P_1^0$ peaks, occurred at slightly higher energies than the $^3P_1^0$ states, and had nearly constant quantum defect, $\delta \approx 3.78$. Above $n = 23$, the $^3P_1^0$ states could not be resolved from the stronger $^3P_2^0$ states in the excitation spectra from the $^3S_1$. In general, the $6snp\ ^3P_0^0$ states were not seen; an exception was the partially resolved $6s16p\ ^3P_0^0$ state.

One other series of lines was seen when the spectrum was observed excited *via* $^3S_1$ but not *via* the $^1S_0$ state. We have identified this series as $6snf\ ^3F_2^0$. It had a relatively constant quantum defect, $\delta \approx 0.17$. It shows a much greater intensity variation than the $^1P_1^0$ and $^3P^0$ series. It is odd parity, must have a 6*s* core (since it converges on the 6*s* limit), and has $J = 0$ or 2. The lowest four members that we observed have energies which agree with Moore's[7] values for $6s9f$ to $6s12f$ $^3F_2^0$. The lines of this series are generally weak, but members of the series centered at $n = 21$ stand out, as indicated by F in Fig. 3. The large peak indicated by P corresponds to an odd parity $J = 2$ state which perturbs the $6snp\ ^3P_2^0$ series as well as the $6snf\ ^3F_2^0$ series.

Scans of the same spectral region made by each of the three methods are shown in Fig. 4. These scans have a common

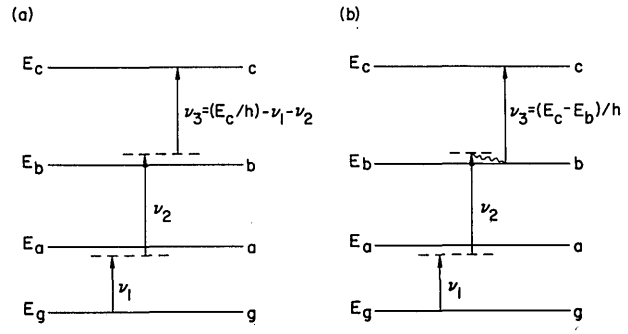

FIG. 5. Three-photon excitation sequences which are (a) fully coherent and (b) incoherent, involving collisional population of level *b*. Each sequence gives rise to a spectral peak, accounting for the splitting of peaks into two when $\nu_1 + \nu_2$ is tuned off resonance with level *b*.

abscissa. The ordinates have a linear scale for the absorption measurement and logarithmic scales for the ionization signal measurements. Note that the $6snp\ ^1P_1^0$ states appear in all three scans and dominate all spectra of high n. This is puzzling for the three-photon excitation spectra *via* the $6s7s\ ^3S_1$ state, where one might expect the $6snp\ ^3P^0$ state to dominate. The explanation is that configuration interaction effects strongly influence the spectra by redistributing oscillator strength from perturbers. These effects are discussed in Sec. IV. Note also the minimum in intensity of the $^1P_1^0$ states around $n = 32$ and 33 in the three-photon excitation *via* the $6s7s\ ^1S_0$ intermediate state. This minimum is analogous to the type described by Fano in his discussion of the configuration interaction between a discrete state and a continuum in the autoionizing region.[17] The Fano minimum seen in absorption from the ground state occurs around $n = 23$ and 24.[4] For the spectrum from $6s7s\ ^1S_0$, the configuration interaction between the $5d8p\ ^1P_1^0$ configuration and the $6snp$ $^1P_1^0$ channel (see Sec. IV) is the same, but the Fano q parameter[17] is different in magnitude, so that the minimum is shifted in energy. This reflects the fact that q depends on *both* the initial and final states of a transition.

There are many peaks in the three-step excitation spectra of Ba which correspond to neither the $6snp\ ^1P_1^0$ nor the $6snp$ $^3P^0$ states. Several of these extra peaks are associated with the configurations $5d6p$, $5d7p$, $5d8p$, and $5d4f$. But most of them are due to excitation to other series from states populated by collisions. The lower levels of these transitions are states, such as the $5d6p\ ^3P_2^0$ state, which lie near the $6s7s\ ^3S_1$ state and are easily populated by collisions. Since the upper levels of these transitions are not all known, the collision peaks were not readily classified and represented a great source of spectral complexity. However, positive identification of transitions originating from the intentionally populated states ($6s7s\ ^1S_0$ or $^3S_1$) could be made by two methods. First, the collision-peak amplitudes are very sensitive to gas pressure. When Ne buffer gas was added, the size of the collision peaks increased while the other peaks (henceforth called "principal peaks") remained more or less constant in amplitude. This pressure dependence identified most of the collision peaks. Second, when the lasers were slightly detuned from the ν_1 and ν_2 resonances, the principal peaks split into two peaks, one unshifted and the other shifted as functions of ν_3. The collision peaks did not split or shift. The splitting may be understood with reference to Fig. 5. With ν_1 tuned below resonance and ν_2 tuned so that $\nu_1 + \nu_2$ in above resonance, final states (c), such as the $6snp\ ^3P_1^0$, may be excited by a three-photon "coherent" excitation.[18] For such a process, the intermediate states are virtual, and three-photon absorption occurs when $\nu_1 + \nu_2 + \nu_3 = (E_c - E_g)/h$ where h is Planck's constant. Thus, since $\nu_1 + \nu_2 > (E_b - E_g)/h$, $\nu_3 < (E_c - E_b)/h$ and the coherent peak is shifted to lower frequency. At the same time, collisions populate the b state and a peak is seen when $\nu_3 = (E_c - E_b)/h$. The size of this collision peak depends on the population of the (b) state and is therefore strongly pressure dependent. Note that both types of peaks decrease in intensity as one detunes farther from resonance with the intermediate states. In this way, the questionable peaks were tested and the principal peaks positively identified by the occurrence of a split peak upon detuning.

Using detuning in combination with laser polarization, additional information could be obtained about the J of the final states: starting from $J = 0$ and proceeding *via* $J = 1$ intermediates, it can be shown that to reach a final state with $J = 0$ in the absence of depolarizing collisions, each step of the three-step excitation must have a mutually orthogonal polarization. When the laser beams are nearly collinear it is not possible to have mutual orthogonality, since each beam is polarized in the plane perpendicular to the propagation direction. Thus, fully coherent excitation of $J = 0$ states is not allowed. On the other hand, if the first intermediate state ($6s6p\ ^3P_1^0$) is depolarized by collisions, then a coherent two-step excitation from $J = 1$ to $J = 0$ is allowed for orthogonal polarizations. Thus, with ν_2 and ν_3 linearly polarized, ν_1 on

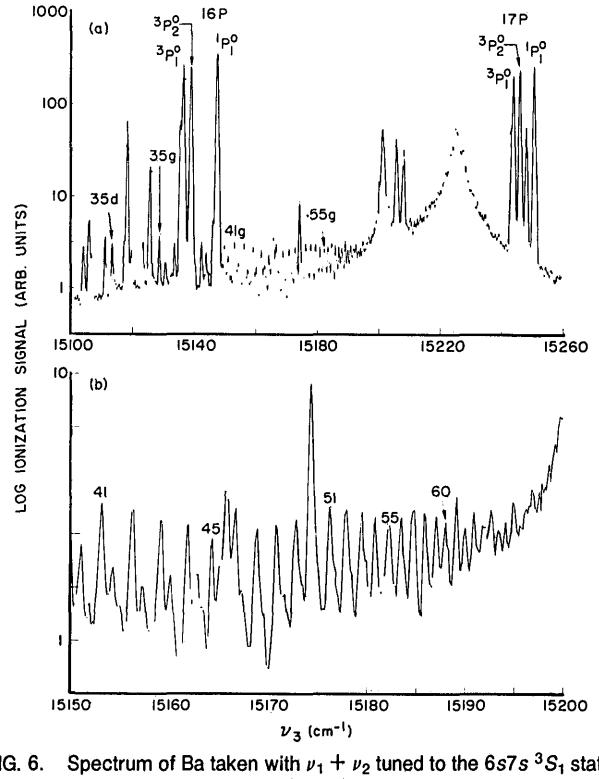

FIG. 6. Spectrum of Ba taken with $\nu_1 + \nu_2$ tuned to the $6s7s\ ^3S_1$ state. The large peaks in (a) are the groups of $6s16p$ and $6s17p$ states. The small peaks are shown on an expanded energy scale in (b) and correspond to transitions from the $5d6p\ ^1F_3^0$ state, populated by collisions, to $6sng\ ^1G_4$ states.

resonance for the $6s^2\ ^1S_0$-$6s6p\ ^3P_1^0$ transition, and ν_2 slightly detuned from the $6s6p\ ^3P_1^0$-$6s7s\ ^3S_1$ transition, the amplitude of a coherent (shifted) peak for a $J = 0$ final state should be strongly polarization dependent. In particular, the coherent peak should be relatively strong for ν_2 polarized perpendicular to ν_3 and relatively weak for ν_2 polarized parallel to ν_3. Several peaks displayed such behavior and were therefore labelled $J = 0$. This was the only method we had to distinguish between $J = 0$ and $J = 2$ states seen in excitation from the $6s7s\ ^3S_1$ state. Of course, $J = 1$ states were distinguishable by also being observed in excitation from $6s^2\ ^1S_0$ or $6s7s\ ^1S_0$. Of the many states we observed in excitation from $6s7s\ ^3S_1$, only two were positively identified as having $J = 0$. These are identified in Sec. III and discussed in Sec. IV E.

Two series were observed converging at a value of ν_3 656 cm^{-1} lower than the convergence value for the series of $6s7s\ ^3S_1$-to-$6snp$ transitions. We identified them as series of collision peaks arising from collisional population of the $5d6p\ ^1F_3^0$ state, located at 26 816.3 cm^{-1}, 656 cm^{-1} above the $6s7s\ ^3S_1$. These series have to have even parity and $J = 2$, 3, or 4. The first of these series corresponds to the recently determined $6snd\ ^1D_2$ states.[19,20] The second does not correspond to the recently observed $6snd\ ^3D_2$ series.[19,20] We assume that spin is preserved in the transition from the $5d6p\ ^1F_3^0$ state and identify this series as $6sng\ ^1G_4$ states. These states have a small and relatively constant quantum defect, $\delta \cong 0.06$. Figure 6 is a scan showing some of these states.

III. ENERGY LEVELS AND IDENTIFICATIONS

Our results for Ca and Sr are quite straightforward. The measured energy values for the newly observed $^3P^0$ states are given in Tables I and II, along with MQDT calculated energies using the parameters of Sec. IV. The $J = 2$ states give the strongest signals, so, when the $J = 0$, 1, and 2 were not resolvable, the measured energy of the unresolved peak was assigned to the $J = 2$ state. We note that the signal perturbers, $3d4p$ in Ca and $4d5p$ in Sr, occur at low energy and

TABLE I. Ca states.

Label		Obs. (cm^{-1})	Calc. (cm^{-1})[a]	Obs. − Calc.	ν_S(Obs.)
$4s4p$	$^3P_0^0$	15 157.90[b]			1.793
$4s4p$	$^3P_1^0$	15 210.06[b]	18 910.43	−3 700.36[c]	1.794
$4s4p$	$^3P_2^0$	15 315.94[b]	19 049.50	−3 733.55[c]	1.797
$4s5p$	$^3P_0^0$	36 547.69[b]			2.933
$4s5p$	$^3P_1^0$	36 554.75[b]	36 721.77	−167.02[c]	2.934
$4s5p$	$^3P_2^0$	36 575.12[b]	36 744.98	−169.86[c]	2.936
$3d4p$	$^3P_0^0$	39 333.38[b]			3.317
$3d4p$	$^3P_1^0$	39 335.32[b]	39 335.32	0.00	3.318
$3d4p$	$^3P_2^0$	39 340.08[b]	39 340.00	0.08	3.318
$4s6p$	$^3P_0^0$	42 514.84[b]			4.020
$4s6p$	$^3P_1^0$	42 518.71[b]	42 518.78	−0.07	4.021
$4s6p$	$^3P_2^0$	42 526.59[b]	42 527.06	−0.47	4.023
$4s7p$	$^3P_0^0$	44 955.67[b]			5.022
$4s7p$	$^3P_1^0$	44 957.65[b]	44 957.66	−0.01	5.024
$4s7p$	$^3P_2^0$	44 961.76[b]	44 961.71	0.05	5.026
$4s8p$	$^3P_0^0$	46 284.12 ± 0.07			6.026
$4s8p$	$^3P_1^0$	46 285.23 ± 0.07	46 285.20	0.03	6.027
$4s8p$	$^3P_2^0$	46 287.63 ± 0.07	46 287.47	0.16	6.030
$4s9p$	$^3P_1^0$	47 085.38 ± 0.07	47 085.30	0.07	7.030
$4s9p$	$^3P_2^0$	47 086.99 ± 0.07	47 086.70	0.28	7.032
$4s10p$	$^3P_1^0$	47 604.75 ± 0.20	47 604.67	0.08	8.031
$4s10p$	$^3P_2^0$	47 605.77 ± 0.20	47 605.60	0.18	8.034
$4s11p$	$^3P_1^0$	47 960.87 ± 0.09	47 960.90	−0.04	9.032
$4s11p$	$^3P_2^0$	47 961.53 ± 0.09	47 961.55	−0.02	9.034
$4s12p$	$^3P_1^0$	48 215.81 ± 0.05	48 215.86	−0.05	10.033
$4s12p$	$^3P_2^0$	48 216.36 ± 0.05	48 216.33	0.03	10.035
$4s13p$	$^3P_1^0$	48 404.57 ± 0.05	48 404.61	−0.04	11.033
$4s13p$	$^3P_2^0$	48 404.95 ± 0.05	48 404.96	−0.01	11.036
$4s14p$	$^3P_1^0$	48 548.30 ± 0.06	48 548.25	0.05	12.034
$4s14p$	$^3P_2^0$	48 548.51 ± 0.06	48 548.52	−0.01	12.036
$4s15p$	$^3P_2^0$	48 660.23 ± 0.05	48 660.30	−0.07	13.036
$4s16p$	$^3P_2^0$	48 749.04 ± 0.05	48 749.05	0.00	14.037
$4s17p$	$^3P_2^0$	48 820.60 ± 0.02	48 820.67	−0.07	15.036
$4s18p$	$^3P_2^0$	48 879.31 ± 0.02	48 879.32	−0.01	16.037
$4s19p$	$^3P_2^0$	48 927.93 ± 0.03	48 927.94	−0.02	17.037
$4s20p$	$^3P_2^0$	48 968.67 ± 0.03	48 968.70	−0.03	18.037
$4s21p$	$^3P_2^0$	49 003.21 ± 0.03	49 003.21	0.00	19.037
$4s22p$	$^3P_2^0$	49 032.70 ± 0.03	49 032.68	0.02	20.038
$4s23p$	$^3P_2^0$	49 058.02 ± 0.03	49 058.05	−0.03	21.037
$4s24p$	$^3P_2^0$	49 080.04 ± 0.03	49 080.04	0.00	22.038
$4s25p$	$^3P_2^0$	49 099.25 ± 0.03	49 099.23	0.02	23.039
$4s26p$	$^3P_2^0$	49 116.07 ± 0.03	49 116.08	−0.01	24.037
$4s27p$	$^3P_2^0$	49 130.94 ± 0.03	49 130.94	0.00	25.038
$4s28p$	$^3P_2^0$	49 144.19 ± 0.03	49 144.13	0.06	26.043
$4s29p$	$^3P_2^0$	49 155.90 ± 0.02	49 155.88	0.01	27.039
$4s30p$	$^3P_2^0$	49 166.43 ± 0.02	49 166.40	0.03	28.041
$4s31p$	$^3P_2^0$	49 175.87 ± 0.02	49 175.85	0.02	29.041
$4s32p$	$^3P_2^0$	49 184.37 ± 0.02	49 184.37	0.00	30.039
$4s33p$	$^3P_2^0$	49 192.08 ± 0.02	49 192.08	0.00	31.038
$4s34p$	$^3P_2^0$	49 199.09 ± 0.02	49 199.08	0.01	32.040
$4s35p$	$^3P_2^0$	49 205.47 ± 0.02	49 205.45	0.02	33.041
$4s36p$	$^3P_2^0$	49 211.34 ± 0.05	49 211.28	0.06	34.049
$4s37p$	$^3P_2^0$	49 216.61 ± 0.02	49 216.60	0.01	35.040
$4s38p$	$^3P_2^0$	49 221.51 ± 0.02	49 221.50	0.02	36.042
$4s39p$	$^3P_2^0$	49 226.02 ± 0.02	49 226.00	0.03	37.044
$4s40p$	$^3P_2^0$	49 230.13 ± 0.02	49 230.15	−0.01	38.034
$4s41p$	$^3P_2^0$	49 234.00 ± 0.02	49 233.98	0.02	39.044
$4s42p$	$^3P_2^0$	49 237.55 ± 0.02	49 237.54	0.02	40.043
$4s43p$	$^3P_2^0$	49 240.81 ± 0.07	49 240.83	−0.02	41.031
$4s44p$	$^3P_2^0$	49 243.87 ± 0.02	49 243.89	−0.02	42.031
$4s45p$	$^3P_2^0$	49 246.74 ± 0.02	49 246.75	−0.01	43.036
$4s46p$	$^3P_2^0$	49 249.37 ± 0.02	49 249.41	−0.04	44.025
$4s47p$	$^3P_2^0$	49 251.87 ± 0.02	49 251.89	−0.02	45.030
$4s48p$	$^3P_2^0$	49 254.22 ± 0.03	49 254.22	0.00	46.039
$4s49p$	$^3P_2^0$	49 256.42 ± 0.02	49 256.39	0.03	47.050
$4s50p$	$^3P_2^0$	49 258.45 ± 0.02	49 258.44	0.01	48.042
$4s51p$	$^3P_2^0$	49 260.36 ± 0.03	49 260.36	0.00	49.039
$4s52p$	$^3P_2^0$	49 262.15 ± 0.03	49 262.16	−0.01	50.032
$4s53p$	$^3P_2^0$	49 263.85 ± 0.03	49 263.86	−0.02	51.029
$4s54p$	$^3P_2^0$	49 265.44 ± 0.03	49 265.47	−0.02	52.024
$4s55p$	$^3P_2^0$	49 266.99 ± 0.03	49 266.98	0.01	53.043
$4s56p$	$^3P_2^0$	49 268.40 ± 0.03	49 268.41	−0.01	54.032
$4s57p$	$^3P_2^0$	49 269.77 ± 0.03	49 269.76	0.00	55.042
$4s58p$	$^3P_2^0$	49 271.01 ± 0.03	49 271.05	−0.04	56.007
$4s59p$	$^3P_2^0$	49 272.24 ± 0.03	49 272.26	−0.02	57.024
$4s60p$	$^3P_2^0$	49 273.37 ± 0.03	49 273.41	−0.04	58.001

[a]Calculated using MQDT parameters given in Table VIII.
[b]From G. Risberg, Ark. Fys. 37, 231 (1968).
[c]Not included in MQDT fit.

TABLE II. Sr states.

Label		Obs. (cm^{-1})	Calc. (cm^{-1})[a]	Obs. − Calc.	ν_S(Obs.)
$5s5p$	$^3P_0^0$	14 317.52[b]	17 812.12	−3 494.60[c]	1.863
$5s5p$	$^3P_1^0$	14 504.35[b]	18 220.00	−3 715.65[c]	1.869
$5s5p$	$^3P_2^0$	14 898.56[b]	19 186.91	−4 288.35[c]	1.880
$5s6p$	$^3P_0^0$	33 853.52[b]	34 000.52	−147.00[c]	3.014
$5s6p$	$^3P_1^0$	33 868.33[b]	34 073.68	−205.34[c]	3.016
$5s6p$	$^3P_2^0$	33 973.08[b]	34 253.73	−280.65[c]	3.029
$4d5p$	$^3P_0^0$	37 292.11[b]	37 292.11	0.00	3.564
$4d5p$	$^3P_1^0$	37 302.76[b]	37 302.77	−0.01	3.566
$4d5p$	$^3P_2^0$	37 336.62[b]	37 336.46	0.15	3.573
$5s7p$	$^3P_0^0$	39 411.70[b]	39 411.62	0.08	4.102
$5s7p$	$^3P_1^0$	39 426.47[b]	39 426.23	0.24	4.107
$5s7p$	$^3P_2^0$	39 457.41[b]	39 458.29	−0.88	4.117
$5s8p$	$^3P_0^0$	41 712.05 ± 0.05	41 712.43	−0.38	5.099
$5s8p$	$^3P_1^0$	41 719.71 ± 0.05	41 720.54	−0.82	5.104
$5s8p$	$^3P_2^0$	41 735.98 ± 0.05	41 738.49	−2.51	5.114
$5s9p$	$^3P_0^0$	42 985.86 ± 0.07	42 985.79	0.08	6.103
$5s9p$	$^3P_1^0$	42 990.26 ± 0.07	42 990.32	−0.07	6.107
$5s9p$	$^3P_2^0$	42 999.79 ± 0.07	43 000.29	−0.49	6.117
$5s10p$	$^3P_0^0$	43 758.65 ± 0.07	43 758.57	0.09	7.105
$5s10p$	$^3P_1^0$	43 761.47 ± 0.07	43 761.35	0.12	7.110
$5s10p$	$^3P_2^0$	43 767.58 ± 0.07	43 767.40	0.18	7.120
$5s11p$	$^3P_0^0$	44 262.70 ± 0.07	44 262.56	0.15	8.107
$5s11p$	$^3P_1^0$	44 264.52 ± 0.07	44 264.38	0.14	8.112
$5s11p$	$^3P_2^0$	44 268.72 ± 0.07	44 268.33	0.39	8.122
$5s12p$	$^3P_0^0$	44 609.51 ± 0.04	44 609.46	0.05	9.109
$5s12p$	$^3P_1^0$	44 610.85 ± 0.04	44 610.72	0.13	9.113
$5s12p$	$^3P_2^0$	44 613.78 ± 0.04	44 613.44	0.34	9.123
$5s13p$	$^3P_0^0$	44 858.33 ± 0.03	44 858.42	−0.09	10.109
$5s13p$	$^3P_1^0$	44 859.32 ± 0.03	44 859.33	−0.01	10.114
$5s13p$	$^3P_2^0$	44 861.46 ± 0.03	44 861.29	0.18	10.124
$5s14p$	$^3P_0^0$	45 043.18 ± 0.02	45 043.14	0.04	11.110
$5s14p$	$^3P_1^0$	45 043.89 ± 0.02	45 043.82	0.07	11.115
$5s14p$	$^3P_2^0$	45 045.54 ± 0.02	45 045.28	0.26	11.125
$5s15p$	$^3P_0^0$	45 183.93 ± 0.02	45 183.97	−0.04	12.110
$5s15p$	$^3P_1^0$	45 184.54 ± 0.02	45 184.49	0.05	12.115
$5s15p$	$^3P_2^0$	45 185.79 ± 0.02	45 185.61	0.19	12.125
$5s16p$	$^3P_1^0$	45 294.22 ± 0.02	45 294.21	0.01	13.115
$5s16p$	$^3P_2^0$	45 295.21 ± 0.02	45 295.08	0.13	13.125
$5s17p$	$^3P_1^0$	45 381.46 ± 0.03	45 381.43	0.04	14.116
$5s17p$	$^3P_2^0$	45 382.26 ± 0.03	45 382.12	0.14	14.126
$5s18p$	$^3P_1^0$	45 451.87 ± 0.01	45 451.91	−0.03	15.115
$5s18p$	$^3P_2^0$	45 452.53 ± 0.01	45 452.47	0.06	15.126
$5s19p$	$^3P_1^0$	45 509.65 ± 0.02	45 509.67	−0.02	16.116
$5s19p$	$^3P_2^0$	45 510.20 ± 0.02	45 510.13	0.07	16.126
$5s20p$	$^3P_1^0$	45 557.62 ± 0.02	45 557.61	0.01	17.116
$5s20p$	$^3P_2^0$	45 558.00 ± 0.02	45 557.99	0.01	17.125
$5s21p$	$^3P_1^0$	45 597.81 ± 0.02	45 597.83	−0.01	18.116
$5s21p$	$^3P_2^0$	45 598.17 ± 0.02	45 598.15	0.02	18.126
$5s22p$	$^3P_1^0$	45 631.86 ± 0.02	45 631.90	−0.04	19.115
$5s22p$	$^3P_2^0$	45 632.15 ± 0.02	45 632.17	−0.02	19.125
$5s23p$	$^3P_2^0$	45 661.22 ± 0.03	45 661.25	−0.03	20.124
$5s24p$	$^3P_2^0$	45 686.25 ± 0.02	45 686.29	−0.04	21.124
$5s25p$	$^3P_2^0$	45 707.96 ± 0.02	45 708.02	−0.06	22.122
$5s26p$	$^3P_2^0$	45 726.94 ± 0.02	45 726.99	−0.05	23.123
$5s27p$	$^3P_2^0$	45 743.60 ± 0.02	45 743.65	−0.05	24.122
$5s28p$	$^3P_2^0$	45 758.33 ± 0.02	45 758.36	−0.02	25.124
$5s29p$	$^3P_2^0$	45 771.41 ± 0.02	45 771.41	0.00	26.126
$5s30p$	$^3P_2^0$	45 782.99 ± 0.02	45 783.05	−0.06	27.120
$5s31p$	$^3P_2^0$	45 793.45 ± 0.02	45 793.46	−0.01	28.124
$5s32p$	$^3P_2^0$	45 802.83 ± 0.02	45 802.83	0.01	29.126
$5s33p$	$^3P_2^0$	45 811.27 ± 0.02	45 811.27	0.00	30.125
$5s34p$	$^3P_2^0$	45 818.91 ± 0.02	45 818.92	−0.01	31.124
$5s35p$	$^3P_2^0$	45 825.83 ± 0.02	45 825.86	−0.03	32.121
$5s36p$	$^3P_2^0$	45 832.16 ± 0.02	45 832.18	−0.02	33.122
$5s37p$	$^3P_2^0$	45 837.93 ± 0.02	45 837.96	−0.03	34.121
$5s38p$	$^3P_2^0$	45 843.22 ± 0.02	45 843.25	−0.03	35.121
$5s39p$	$^3P_2^0$	45 848.05 ± 0.02	45 848.10	−0.05	36.115
$5s40p$	$^3P_2^0$	45 852.56 ± 0.02	45 852.57	−0.01	37.123
$5s41p$	$^3P_2^0$	45 856.68 ± 0.02	45 856.69	−0.01	38.122
$5s42p$	$^3P_2^0$	45 860.54 ± 0.02	45 860.50	0.03	39.135
$5s43p$	$^3P_2^0$	45 864.04 ± 0.02	45 864.03	0.01	40.128
$5s44p$	$^3P_2^0$	45 867.26 ± 0.02	45 867.30	−0.04	41.113
$5s45p$	$^3P_2^0$	45 870.30 ± 0.03	45 870.35	−0.05	42.108
$5s46p$	$^3P_2^0$	45 873.13 ± 0.03	45 873.18	−0.05	43.106
$5s47p$	$^3P_2^0$	45 875.77 ± 0.03	45 875.83	−0.06	44.102
$5s48p$	$^3P_2^0$	45 878.26 ± 0.03	45 878.30	−0.03	45.112
$5s49p$	$^3P_2^0$	45 880.56 ± 0.02	45 880.61	−0.04	46.106
$5s50p$	$^3P_2^0$	45 882.75 ± 0.02	45 882.77	−0.02	47.115
$5s51p$	$^3P_2^0$	45 884.82 ± 0.02	45 884.81	0.01	48.130
$5s52p$	$^3P_2^0$	45 886.71 ± 0.02	45 886.72	−0.01	49.122
$5s53p$	$^3P_2^0$	45 888.43 ± 0.03	45 888.51	−0.08	50.081
$5s54p$	$^3P_2^0$	45 890.18 ± 0.02	45 890.20	−0.02	51.113
$5s55p$	$^3P_2^0$	45 891.80 ± 0.03	45 891.80	0.00	52.128
$5s56p$	$^3P_2^0$	45 893.28 ± 0.02	45 893.31	−0.02	53.111
$5s57p$	$^3P_2^0$	45 894.70 ± 0.02	45 894.73	−0.03	54.103
$5s58p$	$^3P_2^0$	45 896.01 ± 0.02	45 896.08	−0.06	55.076
$5s59p$	$^3P_2^0$	45 897.30 ± 0.02	45 897.35	−0.05	56.084
$5s60p$	$^3P_2^0$	45 898.50 ± 0.02	45 898.56	−0.06	57.078

[a]Calculated using MQDT parameters in Table VIII.
[b]From Ref. 6.
[c]Not included in MQDT fit.

interact only with a small number of *msnp* state *via* the configuration interaction.

The results for Ba are complicated by many perturbers. Tables III–VII give the measured energies of the Ba states, along with configurational labels, effective quantum numbers ν_S, and MQDT energies calculated using the parameters of Sec. IV. Tables III–VI contain odd parity, $J = 0, 1, 2$, and 3 states. Table VII contains even parity, $J = 4$ states.

Note that, in Table IV, the energies for the $6snp\ ^1P_1^0$ states with $n = 10$–12 are substantially revised from Ref. 7. We observed the $6s10p\ ^1P_1^0$ state in absorption and calibrated it against the Na absorption lines. The $6s11p$ and $6s12p\ ^1P_1^0$ states were seen both in absorption and in excitation from the $6s7s\ ^3S_1$ state.

We have revised the ionization limit of Ba down from the value of Garton and Tomkins[4] by 0.24 cm^{-1}, to $I_S = 42\ 034.90 \pm 0.05\ cm^{-1}$. We have been led to this because our MIS techniques provide us two series, $^3P_2^0$ and $^1G_4$, which we find to be essentially unperturbed. That is, both series go asymptotically to I_S with constant quantum defects once the new I_S is adopted.

TABLE III. Ba $^3P_0^0$ states.

Label	Observed (cm^{-1})	ν_S (Obs.)
$5d8p$	41 083.92 ± 0.15	10.742
$6s16p$	41 295.93 ± 0.15	12.186

IV. MQDT ANALYSIS

A. General comments

The tool used in our analysis is the multichannel quantum defect theory (MQDT), due originally to Seaton and coworkers[21] with more recent elaboration by Fano and coworkers.[8] Within the range of its applicability, MQDT is essentially an exact parametrization of the energy levels and wave functions of interacting Rydberg series. Since it treats whole series in a unified way, it is often superior to conventional analysis based on one-electron configurations supplemented by the use of perturbation theory on a level-by-level basis.

The MQDT is not a perturbation method. Rather it is based on the fact that a highly excited electron sees a Coulomb potential during most of its orbit and hence has an analytically known wave function for that part of the orbit. The wave function is a linear combination of regular and irregular Coulomb wave functions. The theory is parametrized in

TABLE IV. Ba, odd-parity, $J = 1$ states.

Label		Obs. (cm^{-1})	Calc. (cm^{-1})[a]	Obs. − Calc.	ν_S(Obs.)	Label		Obs. (cm^{-1})	Calc. (cm^{-1})[a]	Obs. − Calc.	ν_S(Obs.)
$6s6p$	^3P	12 636.616[b]			1.932	$6s27p$	^1P	41 830.03 ± 0.02	41 829.96	0.06	23.144
$6s6p$	^1P	18 060.264[b]			2.140	$6s27p$	^3P	41 830.94 ± 0.04	41 830.97	−0.03	23.196
$5d6p$	^3D	24 192.057[b]	23 381.5	−853[c]	2.480	$6s28p$	^1P	41 846.48 ± 0.04	41 846.38	0.10	24.133
$5d6p$	^3P	25 704.14[b]	25 828.1	−114[c]	2.592	$6s28p$	^3P	41 847.45 ± 0.04	41 847.47	−0.02	24.195
$5d6p$	^1P	28 554.257[b]	28 554.04	0.21	2.853	$6s29p$	^1P	41 860.99 ± 0.05	41 860.89	0.10	25.120
$6s7p$	^3P	30 815.562[b]	30 815.80	−0.24	3.127	$6s29p$	^3P	41 862.03 ± 0.04	41 862.05	−0.02	25.195
$6s7p$	^1P	32 547.076[b]	32 547.40	−0.32	3.401	$6s30p$	^1P	41 873.88 ± 0.02	41 873.79	0.10	26.106
$6s8p$	^3P	35 669.00 ± 0.20	35 669.60	−0.60	4.152	$6s30p$	^3P	41 874.97 ± 0.04	41 875.00	−0.03	26.195
$6s8p$	^1P	35 892.52[b]	35 892.45	0.07	4.227	$6s31p$	^1P	41 885.39 ± 0.03	41 885.29	0.10	27.092
$5d7p$	^3D	36 495.62 ± 0.10	36 495.62	0.00	4.451	$6s31p$	^3P	41 886.48 ± 0.04	41 886.54	−0.06	27.191
$5d7p$	^3P	36 989.98 ± 0.10	36 989.98	0.00	4.664	$6s32p$	^1P	41 895.70 ± 0.03	41 895.61	0.09	28.077
$6s9p$	^1P	37 775.28 ± 0.06	37 776.06	−0.78	5.076	$6s32p$	^3P	41 896.85 ± 0.04	41 896.87	−0.02	28.194
$6s9p$	^3P	37 936.87 ± 0.08	37 935.58	1.29	5.175	$6s33p$	^1P	41 905.03 ± 0.03	41 904.89	0.14	29.068
$5d7p$	^1P	38 500.29 ± 0.09	38 500.44	−0.15	5.572	$6s33p$	^3P	41 906.12 ± 0.04	41 906.17	−0.05	29.191
$6s10p$	^3P	39 160.21 ± 0.15	39 159.41	0.80	6.178	$6s34p$	^1P	41 913.39 ± 0.02	41 913.28	0.11	30.052
$6s10p$	^1P	39 311.95 ± 0.15	39 310.36	1.59	6.348	$6s34p$	^3P	41 914.55 ± 0.04	41 914.55	0.00	30.196
$5d4f$	(d)	39 893.48 ± 0.07	39 893.45	0.03	7.159	$6s35p$	^1P	41 921.00 ± 0.02	41 920.88	0.12	31.039
$6s11p$	^3P	39 916.35 ± 0.07	39 916.24	0.11	7.197	$6s35p$	^3P	41 922.13 ± 0.04	41 922.14	−0.01	31.195
$6s11p$	^1P	39 982.14 ± 0.07	39 980.79	1.35	7.312	$6s36p$	^1P	41 927.90 ± 0.03	41 927.79	0.11	32.025
$6s12p$	^3P	40 395.60 ± 0.07	40 396.04	−0.44	8.182	$6s36p$	^3P	41 929.02 ± 0.04	41 929.04	−0.02	32.194
$6s12p$	^1P	40 428.68 ± 0.06	40 427.41	1.27	8.266	$6s37p$	^1P	41 934.18 ± 0.02	41 934.09	0.09	33.008
$5d4f$	(d)	40 662.86 ± 0.18	40 662.86	0.00	8.943	$6s37p$	^3P	41 935.34 ± 0.04	41 935.32	0.02	33.200
$6s13p$	^3P	40 732.01 ± 0.12	40 731.96	0.05	9.177	$6s38p$	^1P	41 939.95 ± 0.02	41 939.85	0.10	33.996
$5d4f$	(d)	40 736.81 ± 0.15	40 736.80	0.01	9.194	$6s38p$	^3P	41 940.99 ± 0.04	41 941.06	−0.07	34.184
$6s13p$	^1P	40 765.23 ± 0.14	40 765.32	−0.09	9.297	$6s39p$	^1P	41 945.20 ± 0.02	41 945.14	0.06	34.977
$5d8p$	^3D	40 893.76 ± 0.13	40 893.76	0.00	9.806	$6s39p$	^3P	41 946.27 ± 0.05	41 946.32	−0.05	35.187
$6s14p$	^3P	40 973.65 ± 0.07	40 973.58	0.07	10.169	$6s40p$	^1P	41 950.07 ± 0.04	41 949.99	0.08	35.967
$6s14p$	^1P	40 991.23 ± 0.09	40 990.34	0.89	10.254	$6s40p$	^3P	41 951.10 ± 0.04	41 951.14	−0.04	36.187
$5d8p$	^3P	41 097.20 ± 0.07	41 097.18	0.02	10.818	$6s41p$	^1P	41 954.55 ± 0.02	41 954.47	0.08	36.956
$6s15p$	^3P	41 159.83 ± 0.12	41 160.11	−0.28	11.198	$6s41p$	^3P	41 955.62 ± 0.06	41 955.59	0.03	37.204
$6s15p$	^1P	41 183.60 ± 0.06	41 184.81	−1.21	11.354	$6s42p$	^1P	41 958.68 ± 0.02	41 958.60	0.08	37.944
$6s16p$	^3P	41 296.96 ± 0.03	41 297.09	−0.13	12.195	$6s43p$	^1P	41 962.43 ± 0.04	41 962.43	0.00	38.913
$6s16p$	^1P	41 307.88 ± 0.03	41 308.69	0.81	12.286	$6s43p$	^3P	41 963.48 ± 0.04	41 963.47	0.01	39.198
$6s17p$	^3P	41 404.40 ± 0.03	41 404.57	−0.17	13.193	$6s44p$	^1P	41 966.03 ± 0.02	41 965.97	0.06	39.917
$6s17p$	^1P	41 411.04 ± 0.03	41 411.67	−0.63	13.263	$6s45p$	^1P	41 969.32 ± 0.02	41 969.26	0.06	40.906
$6s18p$	^3P	41 490.09 ± 0.02	41 490.22	−0.13	14.192	$6s46p$	^1P	41 972.36 ± 0.02	41 972.33	0.03	41.889
$6s18p$	^1P	41 494.39 ± 0.02	41 494.48	−0.43	14.249	$6s47p$	^1P	41 975.21 ± 0.02	41 975.18	0.03	42.877
$6s19p$	^3P	41 559.45 ± 0.03	41 559.53	−0.08	15.192	$6s48p$	^1P	41 977.87 ± 0.02	41 977.85	0.02	43.866
$6s19p$	^1P	41 562.24 ± 0.02	41 562.53	−0.29	15.237	$6s49p$	^1P	41 980.35 ± 0.02	41 980.34	0.01	44.852
$6s20p$	^3P	41 616.32 ± 0.02	41 616.41	−0.09	16.192	$6s50p$	^1P	41 982.71 ± 0.02	41 982.68	0.03	45.855
$6s20p$	^1P	41 618.12 ± 0.02	41 618.32	−0.20	16.226	$6s51p$	^1P	41 984.90 ± 0.02	41 984.86	0.04	46.848
$6s21p$	^3P	41 663.55 ± 0.03	41 663.63	−0.08	17.190	$6s52p$	^1P	41 986.94 ± 0.02	41 986.92	0.02	47.834
$6s21p$	^1P	41 664.66 ± 0.02	41 664.82	−0.16	17.216	$6s53p$	^1P	41 988.89 ± 0.02	41 988.85	0.04	48.837
$6s22p$	^3P	41 703.25 ± 0.02	41 703.25	0.00	18.190	$6s54p$	^1P	41 990.68 ± 0.02	41 990.67	0.01	49.816
$6s22p$	^1P	41 703.84 ± 0.02	41 703.98	−0.14	18.206	$6s55p$	^1P	41 992.40 ± 0.02	41 992.38	0.02	50.814
$6s23p$	^1P	41 736.80 ± 0.03	41 736.77	0.03	19.186						
$6s24p$	^1P	41 765.35 ± 0.02	41 765.34	0.01	20.177						
$6s25p$	^1P	41 789.99 ± 0.02	41 789.94	0.05	21.168						
$6s26p$	^1P	41 811.34 ± 0.02	41 811.30	0.04	22.155						
$6s26p$	^3P	41 812.03 ± 0.06	41 812.19	−0.16	22.190						

[a] Calculated using MQDT parameters in Table XIV.
[b] From Ref. 7.
[c] Not included in MQDT fit.
[d] Russell-Saunders notation is not appropriate for the $5d4f$ states. See Table XVI for proper labelling.

TABLE V. Ba $^3P_2^0$ states.

Label	Obs. (cm^{-1})	Calc. (cm^{-1})[a]	Obs. − Calc.	ν_S(Obs.)
$6s11p$	39 930.79 ± 0.19	39 922.22	8.57[b]	7.222
$6s12p$	40 406.67 ± 0.19	40 406.76	−0.09	8.210
$6s13p$	40 741.76 ± 0.17	40 741.66	0.10	9.212
$6s14p$	40 982.86 ± 0.15	40 982.82	0.04	10.213
$6s15p$	41 162.15 ± 0.15	41 162.25	−0.10	11.213
$6s16p$	41 299.33 ± 0.15	41 299.38	−0.05	12.214
$6s17p$	41 406.53 ± 0.15	41 406.53	0.00	13.215
$6s18p$	41 491.80 ± 0.04	41 491.85	−0.05	14.215
$6s19p$	41 560.83 ± 0.03	41 560.90	−0.07	15.214
$6s20p$	41 617.51 ± 0.03	41 617.55	0.04	16.215
$6s21p$		41 664.60		17.215[a]
$6s22p$		41 704.09		18.213[a]
$6s23p$	41 737.39 ± 0.03	41 737.46	−0.07	19.205
perturber[c]	41 759.93 ± 0.03	41 759.95	−0.02	19.977
$6s24p$	41 767.32 ± 0.03	41 767.36	−0.04	20.251
$6s25p$	41 791.29 ± 0.03	41 791.32	−0.03	21.224
$6s26p$	41 812.66 ± 0.03	41 812.69	−0.03	22.221
$6s27p$	41 831.38 ± 0.03	41 831.40	−0.02	23.221
$6s28p$	41 847.80 ± 0.03	41 847.84	−0.04	24.218
$6s29p$	41 862.37 ± 0.03	41 862.38	−0.01	25.220
$6s30p$	41 875.26 ± 0.03	41 875.29	−0.03	26.218
$6s31p$	41 886.78 ± 0.03	41 886.80	−0.02	27.219
$6s32p$	41 897.11 ± 0.03	41 897.11	0.00	28.221
$6s33p$	41 906.36 ± 0.03	41 906.38	−0.02	29.218
$6s34p$	41 914.71 ± 0.03	41 914.74	−0.03	30.216
$6s35p$	41 922.30 ± 0.03	41 922.31	−0.01	31.218
$6s36p$	41 929.18 ± 0.03	41 929.19	−0.01	32.218
$6s37p$	41 935.44 ± 0.03	41 935.46	−0.02	33.216
$6s38p$	41 941.18 ± 0.03	41 941.19	−0.01	34.218
$6s39p$	41 946.41 ± 0.03	41 946.43	−0.02	35.215
$6s40p$	41 951.25 ± 0.03	41 951.25	0.00	36.220
$6s41p$	41 955.67 ± 0.03	41 955.69	−0.02	37.216
$6s42p$	41 959.76 ± 0.03	41 959.78	−0.02	38.216
$6s43p$	41 963.56 ± 0.03	41 963.56	0.00	39.220
$6s44p$	41 967.05 ± 0.03	41 967.06	−0.01	40.216
$6s45p$	41 970.43 ± 0.11	41 970.31	0.12	41.257
$6s46p$	41 973.32 ± 0.03	41 973.34	−0.02	42.214
$6s47p$	41 976.09 ± 0.06	41 976.15	−0.06	43.197
$6s48p$	41 978.76 ± 0.03	41 978.78	−0.02	44.212
$6s49p$	41 981.21 ± 0.03	41 981.24	−0.03	45.209
$6s50p$	41 983.45 ± 0.05	41 983.53	−0.08	46.183
$6s51p$	41 985.67 ± 0.03	41 985.68	−0.01	47.213
$6s52p$	41 987.69 ± 0.04	41 987.70	−0.01	48.212
$6s53p$	41 989.54 ± 0.04	41 989.60	−0.06	49.186
$6s54p$	41 991.38 ± 0.04	41 991.39	−0.01	50.215

[a]Calculated using MQDT parameters in Table XVII.
[b]Not included in MQDT fit.
[c]This state is tentatively labelled $5d8p\ ^3P_2^0$. See text in Sec. IV E.

TABLE VI. Ba $^3F_2^0$ states.

Label	Obs. (cm^{-1})	ν_S(Obs.)
$6s9f$	40 613.87 ± 0.18	8.788
$6s10f$	40 895.14 ± 0.15	9.812
$6s11f$	41 100.72 ± 0.22	10.838
$6s12f$	41 251.16 ± 0.34	11.833
$6s17f$	41 647.85 ± 0.03	16.838
$6s18f$	41 689.80 ± 0.03	17.832
$6s19f$	41 725.39 ± 0.03	18.830
$6s20f$	41 755.48 ± 0.03	19.817
$6s21f$	41 782.02 ± 0.03	20.831
$6s22f$	41 804.59 ± 0.03	21.828
$6s23f$	41 824.30 ± 0.03	22.827
$6s24f$	41 841.63 ± 0.04	23.828
$6s25f$	41 856.85 ± 0.04	24.826

terms of a small number of physically meaningful quantities, namely, the elements of a unitary transformation matrix $U_{i\alpha}$ and the eigenquantum defects μ_α.

The unitary matrix $U_{i\alpha}$ specifies the transformation which diagonalizes the scattering matrix for the non-Coulomb part of the scattering of the excited electron by the ion core. This unitary transformation transforms the basis set of "collision" channels to a basis set of "close-coupling" channels. In general, a channel encompasses both a region of discrete energies and a continuum. A collision (i) channel describes a set of states that consists of an outer electron with various energy and a core in a definite energy level. Specification of the angular momenta of the outer electron and of the core, along with their coupling, completes description of the channel. The set of states forming a collision channel does not diagonalize the electron-electron part of the Hamiltonian. However, the alternate set of "close-coupling" (α) channels does diagonalize the noncentral part of the electron-electron interaction. The eigendefects μ_α are related to the eigenvalues $[\exp(i2\pi\mu_\alpha)]$ of the scattering matrix and are $1/\pi$ times the phase shift, due to the core, experienced by an electron in an α channel.

Furthermore, MQDT assigns to each observed energy level E as many effective, principal quantum numbers ν_i as there are relevant series limits. (These ν_i are not to be confused with the laser frequencies mentioned earlier.) Thus we determine the ν_i from $E = I_i - \mathrm{R}/(\nu_i)^2$ where I_i is the ith series limit and R is the Rydberg constant. The graphical presentation of MQDT is in terms of plots of $\mu_i = -\nu_i \pmod 1$ *vs* $\nu_j \pmod 1$. These are called Lu-Fano plots.

This section describes the MQDT analysis of the data of Sec. III. Although we present analyses of Ca and Sr as well, this section emphasizes the case of Ba. The analysis is important in Ba for several reasons. First, it has helped to sort out and identify the new $J = 1$, odd states from hundreds of other, non-$J = 1$, states seen in the three-laser, multiphoton ionization spectra. Second, because there are three bound states in each perturbing channel, the Ba $J = 1$ odd spectrum offers the best test to-date of MQDT on interpenetrating series which interact primarily by configuration interaction rather than by spin-orbit interaction (as is the case in the rare-gas spectra[22,23]). The Ca and Sr $J = 1$, odd spectra (to be analyzed below) have only one bound member of each perturbing channel (e.g., $3d4p$ in Ca, $4d5p$ in Sr). In Ba, on the other hand, the three series ^3D, ^3P, ^1P from $5dnp$ each have three members in the bound region. This is a much more demanding case for MQDT analysis. Furthermore, the substantial data on the bound parts of the $5dnp$ channels and their interaction with the $6snp$ channels allows, as the cases of Ca and Sr do not, real hope of "predicting" the Ba $J = 1$, odd, autoionizing spectra. This comparison will be reported in a separate paper.[24] Finally, our MQDT analysis of the Ba $J = 1$, odd spectrum has revealed the first case in which energy-dependent interaction angles[23] are required to fit bound-state data. This carries over into the description of

TABLE VII. Ba $^1G_4$ states.

Label	Obs. (cm^{-1})[a]	ν_S(Obs.)
6s12g	41 265.70	11.94
6s13g	41 379.93	12.94
6s14g	41 470.46	13.94
6s15g	41 543.82	14.95
6s17g	41 652.59	16.94
6s18g	41 693.99	17.94
6s19g	41 729.31	18.95
6s21g	41 784.65	20.94
6s22g	41 806.88	21.94
6s23g	41 826.33	22.94
6s24g	41 843.49	23.94
6s25g	41 858.51	24.94
6s26g	41 871.78	25.94
6s27g	41 883.73	26.94
6s29g	41 903.89	28.94
6s30g	41 912.54	29.95
6s31g	41 920.27	30.94
6s32g	41 927.40	31.95
6s34g	41 939.58	33.93
6s35g	41 945.04	34.95
6s36g	41 949.94	35.94
6s38g	41 958.70	37.95
6s40g	41 966.12	39.94
6s41g	41 969.41	40.94
6s42g	41 972.55	41.95
6s43g	41 975.43	42.96
6s44g	41 978.14	43.97
6s45g	41 980.62	44.96
6s46g	41 982.96	45.97
6s47g	41 985.17	46.98
6s48g	41 987.24	47.98
6s49g	41 989.16	48.98
6s51g	41 992.62	50.94
6s52g	41 994.26	51.96
6s53g	41 995.87	53.02
6s54g	41 997.23	53.97
6s55g	41 998.64	55.01
6s56g	41 999.84	55.95
6s57g	42 001.08	56.97
6s58g	42 002.31	58.03
6s59g	42 003.42	59.04
6s60g	42 004.35	59.93
6s62g	42 006.31	61.96
6s63g	42 007.23	62.97
6s64g	42 008.22	64.13
6s65g	42 008.95	65.03
6s66g	42 009.76	66.06
6s67g	42 010.43	66.97
6s68g	42 011.30	68.18

[a]This data was extracted from a single spectral scan with an estimated accuracy of ± 0.34 cm^{-1}.

autoionizing spectra as well, and explains[24] the anomalous[25] linewidths of the first few ^1P autoionizing line of Ca, Sr, and Ba.

The reader should not expect to completely understand how the following analyses were done unless he reads Refs. 8, 14, and 23. This is particularly true with respect to the complex case of Ba. In addition to reading these references, the reader should try his own hand at MQDT analysis if he wishes to appreciate the details.

B. Calcium and strontium

The $4snp$ series of Ca is perturbed by $3d4p$, and the $5snp$ series of Sr is perturbed by $4d5p$. The spin-orbit interaction in the bound region of the spectrum is so weak that singlets and triplets may be treated separately. We present the two-channel MQDT analyses of both singlets and triplets in Ca and Sr. The singlet term values are not new but are taken from the literature.[26] The case of Sr $5snp$ $^1P_1^0$ has already been published[3,25] but we repeat it here (with slightly revised parameters) for completeness. The MQDT analysis for Ca $4snp$ $^1P_1^0$ is presented here for the first time. The analyses for the Ca and Sr triplets are more thorough than the preliminary results published earlier.[9]

The two-channel fits are found to require four parameters, the eigenquantum defects μ_1 and μ_2, a single energy dependence $d\mu_1/dE$, and the one independent element (U_{21}) of the unitary matrix $U_{i\alpha}$. The ionization limits are taken from Refs. 1 and 3 for Ca and Sr, respectively. The collision (i) channels have the configurations $4snp$ and $3dnp$ for Ca, and $5snp$ and $4dnp$ for Sr. These channels are mixed by the U matrix to give the close-coupled (α) channel description. *The i channels and α channels are both taken as Russell-Saunders coupled, with L and S as good quantum numbers.* Thus for example, the $^1P_1^0$ problem is treated independently of $^3P_1^0$. The physical reasons for doing this are that (i) the lowest ionization limit ($^2S_{1/2}$) corresponds to a core with no spin-orbit splitting since $L = 0$ and (ii) the next relevant limits ($^2D_{3/2,5/2}$) have a spin-orbit splitting which is small in comparison to their separation from the bound states. As we shall see, the latter situation does not apply to Ba, with the consequence that the collision channels are appropriately described by jj coupling.

TABLE VIII. Two-Channel MQDT parameters for Ca and Sr.

		Ca	Sr
Ionization Limit	I_S	49 305.99 cm^{-1}	45 932.19 cm^{-1}
	I_D	63 016.93 cm^{-1}	60 628.26 cm^{-1}
$^1P_1^0$	μ_1	0.965 9(1)[a] + 0.213(1)dE[b]	0.892 2(2) + 0.257 8(7)dE
	μ_2	0.566 13(1)	0.490 66(4)
	U_{21}	0.557 69(7)	0.576 5(2)
$^3P_0^0$	μ_1	...	0.900 0(3) + 0.266 (8)dE
	μ_2	...	0.810 4(7)
	U_{21}	...	0.444 (4)
$^3P_1^0$	μ_1	0.972 5(5) + 0.24(1)dE	0.896 1(5) + 0.25(1)dE
	μ_2	0.838 0(7)	0.810 (1)
	U_{21}	0.31(1)	0.411 (6)
$^3P_2^0$	μ_1	0.971(1) + 0.24(2)dE	0.887 (2) + 0.20(3)dE
	μ_2	0.838 (2)	0.810 (3)
	U_{21}	0.31(3)	0.42(2)

[a]Probable error in last digit shown in parentheses.
[b]Linearly energy-dependent eigendefect where $dE = (I_S - E)/I_S$.

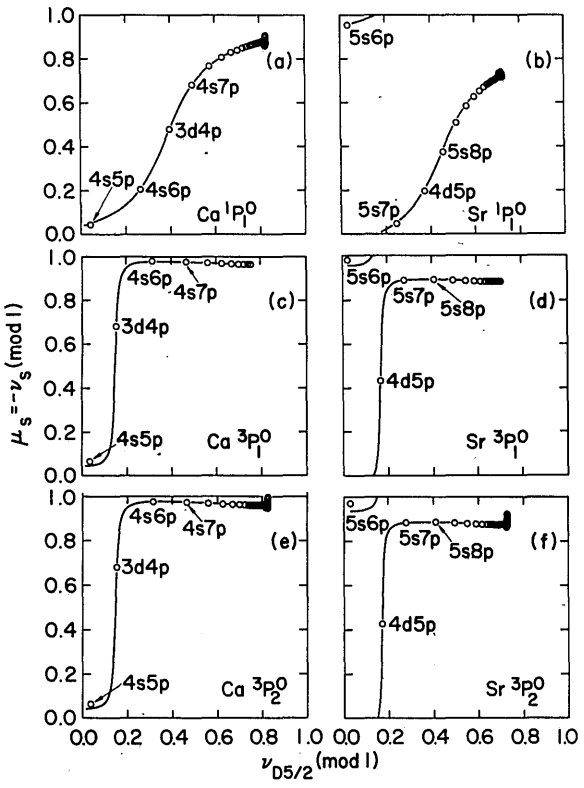

FIG. 7. Lu-Fano plots of odd-parity $4snp$ and $5snp$ series in Ca and Sr respectively. The open circles are experimental data points, and the solid lines are MQDT fit theoretical curves using the parameters in Table VIII.

The MQDT parameters were determined by least-squares fits to the data. The values of the parameters given by these fits are presented in Table VIII. Figure 7 gives Lu-Fano plots of the data and the MQDT fits. Note the similarities between Ca and Sr. The configuration interactions are almost identical for the $^1P_1^0$ channels. The main difference between Ca and Sr is a displacement of both μ_1 and μ_2 by ~ -0.075 from Ca to Sr. Figure 7 shows a much smaller configuration interaction in the triplets as compared to the singlets. The goodness of the MQDT parametrizations are seen as follows. For Ca, all but the two lowest ($4s4p$ and $4s5p$) states were fit. For the $^1P_1^0$, $^3P_1^0$, and $^3P_2^0$ states, the average errors are 0.02, -0.002, and -0.003 cm^{-1} and the rms errors are 0.06, 0.05, 0.08 cm^{-1}, respectively. For Sr $^1P_1^0$ all but the lowest ($5s5p$) state was fit and the average error is -0.03 cm^{-1} while the rms error is 0.15 cm^{-1}. For Sr $^3P_0^0$, $^3P_1^0$, and $^3P_2^0$, all but the two lowest ($5s5p$ and $5s6p$) states were fit. For the $^3P_0^0$, $^3P_1^0$, and $^3P_2^0$ states, the average errors are 0.004, 0.01, and 0.05 cm^{-1} and the rms errors are 0.14, 0.22, 0.38 cm^{-1}, respectively. We note an anomalously large discrepancy between experiment and theory for the Sr $5s8p$ $^3P_1^0$ and $^3P_2^0$ states.

A slight downward slope of the theoretical curves on the right-hand portions of Figs. 7(c–f) is noticeable. This is due to the energy dependence of μ_1. The singlets have comparable energy dependence, but it is not noticeable from Figs. 7(a), 7(b) because of the larger configuration interaction. The scatter of μ_S for the higher-lying states in Figs. 7(a), 7(b), 7(e), and 7(f) reflects the experimental error in the term values and its increasing effect on μ_s as E approaches the I_S limit.

Finally, where $^3P_0^0$, $^3P_1^0$, and $^3P_2^0$ states were resolved, the intervals were measured and their ratios $(^3P_2^0 - {}^3P_1^0)/(^3P_1^0 - {}^3P_0^0)$ determined. These ratios, approximately 2.07 and 2.19 in Ca and Sr, respectively, are close to the value 2 expected for pure Russell-Saunders coupling. These invervals, together with the observed separations of $^1P_1^0$ and $^3P_1^0$ states, result in estimates of $a^2 \sim 10^{-4}$ and $\sim 10^{-3}$ for Ca and Sr, respectively, where a is defined by $\psi = \psi(^1P_1^0) + a\psi(^3P_1^0)$.

C. Barium, $J = 1$

An MQDT treatment of Ba begins with identification of the important interacting channels and the relevant series limits. In addition to the three, $5dnp$ perturbing channels, three channels of the $5dnf$ configuration also perturb the spectrum. Each $5dnf$ channel contributes one bound state (two reported for the first time here). Thus, there are eight channels of importance: $6snp$ ^3P, ^1P; $5dnp$ ^3D, ^3P, ^1P; and $5dnf$ ^3D, ^3P, ^1P. Because of the substantial spin-orbit splitting between the $^2D_{3/2}$ and $^2D_{5/2}$ states of Ba^+, there are three series limits of importance: I_S, $I_{D3/2}$, $I_{D5/2}$. Moreover, since the Ba $J = 1$, odd spectrum seems unperturbed by channels involving a $6p$ core, at least up to the $^2D_{5/2}$ threshold,[4] the spectrum really requires *only* a three-limit analysis to reproduce both bound *and* the autoionizing[24] series up to $^2D_{5/2}$. (This seems not to be true for Ca or Sr $J = 1$ odd spectra.[1,2])

Although eight channels are required for a complete description of the bound spectrum, the analysis is best done in two stages. First a five-channel, three-limit treatment is made, describing the $6snp$-$5dnp$ interactions, and leaving out states that are $5d4f$ or states perturbed by $5d4f$. Thus, the first stage does not try to fit the $5d4f$ states at 39 893.48, 40 662.86, and 40 736.81 cm^{-1}, nor the states $6s11p$ ^3P, ^1P at 39 916.35 and 39 982.14 cm^{-1}, nor the states $6s13p$ ^3P, ^1P at 40 732.01 and 40 765.23 cm^{-1}. After the five-channel fit is made to the other states, the excluded states listed above are fit by adding the $5dnf$ channels in an eight-channel, three-limit treatment.

Five-Channel Treatment

In Ref. 14, Sec. III C., we gave a detailed description of the way to apply MQDT to a three-limit problem. We follow that treatment closely and so will not repeat derivations or formulas here.

Three types of channels are needed: (i) the collision, or i channels, which are jj coupled and have pure configurations; (ii) the $\bar{\alpha}$ channels which are pure configurations and have LS coupling; and (iii) the α channels, which are "close-coupled," approximately LS coupled, and of mixed configuration. We follow Ref. 23 in factoring the $U_{i\alpha}$ matrix, so that $U_{i\alpha} = \Sigma\, U^0_{i\bar{\alpha}} V_{\bar{\alpha}\alpha}$. The $U^0_{i\bar{\alpha}}$ is a block-diagonal, pure-configuration, jj-LS coupling matrix[23] and, with the known spin-orbit splittings of the ^2D ionization threshold, accounts for most of the angular momemtum recoupling effects, while $V_{\bar{\alpha}\alpha}$ describes primarily the configuration interactions. The labelling of channels and limits for the five-channel fit is shown in Table IX.

Having enumerated and labelled the channels and limits, the next step in applying MQDT to the data is to obtain rough values for the eigendefects, μ_α. Figure 8 shows all the $J = 1$ odd states from Table IV plotted (a) ($\mu_S = -\nu_S$ mod 1) vs ($\nu_{D5/2}$ mod 1), and (b) ($\mu_S = -\nu_S$ mod 1) vs ($\nu_{D3/2}$ mod 1). From these plots, as described in Sec. III C. of Ref. 14, one can

TABLE IX. MQDT labels for five-channel fit to Ba $J = 1$, odd.

$i, \bar{\alpha}$	=	1	2	3	4	5
$\|i\rangle$	=	$[^2S_{1/2}]p_{1/2}$	$[^2S_{1/2}]p_{3/2}$	$[^2D_{3/2}]p_{1/2}$	$[^2D_{3/2}]p_{3/2}$	$[^2D_{5/2}]p_{3/2}$
I_i	=	42 034.9	42 034.9	46 908.99	46 908.99	47 709.96 cm^{-1}
$\|\bar{\alpha}\rangle$	=	$6snp\ ^3P$	$6snp\ ^1P$	$5dnp\ ^3D$	$5dnp\ ^3P$	$5dnp\ ^1P$

get rough values for eigendefects and an idea of the most important $V_{\bar{\alpha}\alpha}$ elements. The states shown by crosses (+) were known from Refs. 4, 7, 16; the states marked Δ are our new values for low-lying $^1P_1$ states and for $23p$ and $24p$; the states shown by open circles (O) are "new" ^3P states; the states shown by open squares (□) are our identification of the $5d4f$ perturbers. The importance of three limits is shown by the significant differences between the appearance of Figs. 8(a) and 8(b). In Fig. 9 we show the experimental states plotted ($\mu_S = -\nu_S$ mod 1) vs $\nu_{D5/2}$, i.e., without folding back into the unit square.

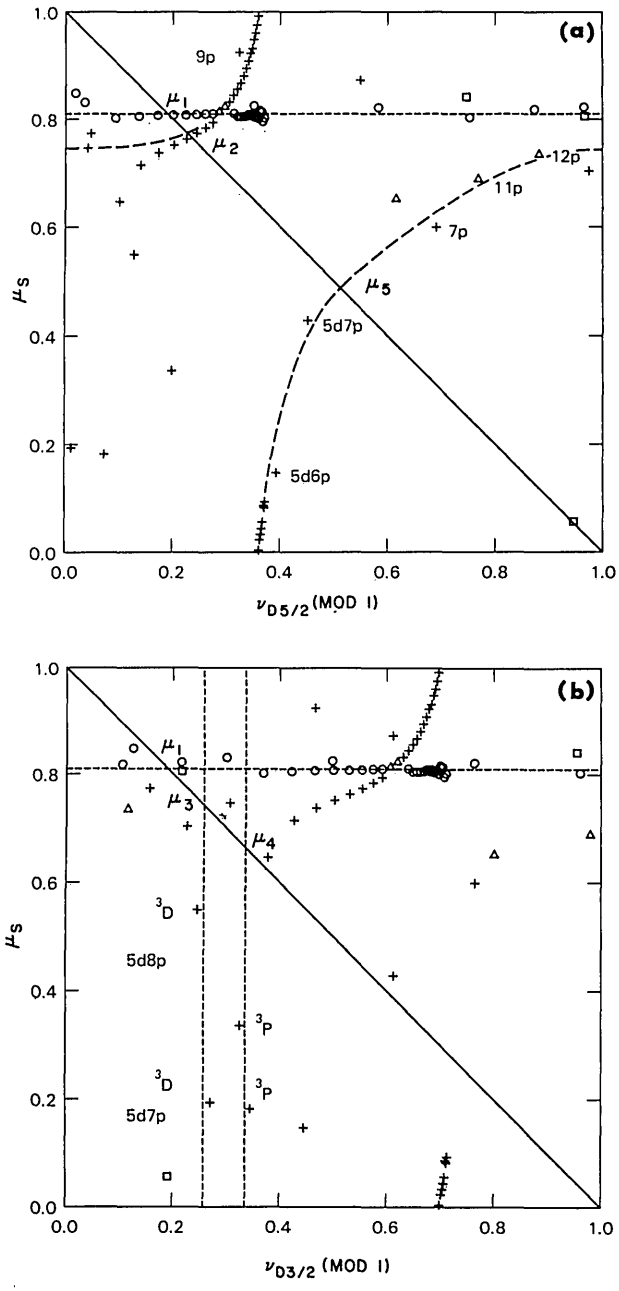

FIG. 8. Lu-Fano plots of odd-parity, $J = 1$ states of Ba. The symbols represent experimental data points with + representing states known from Refs. 4, 7, and 16, Δ representing our new values for ^1P states, O representing "new" ^3P states, *and* □ *representing* $5d4f$ perturbers. The dashed lines are hand-sketched curves connecting states in order of increasing energy.

The dashed lines in Fig. 8 are hand-sketched, tentative curves connecting states of a particular channel and serve to give approximate eigendefects. The μ_α are found from the intersections of the solid diagonal line and the dashed lines.[23] The intersections are labelled, in Fig. 8, by the corresponding μ_α. The clearest case is μ_1, for $6snp\ ^3P$, which is seen from either figure to be about 0.81. Since the strongest perturbation of $6snp\ ^1P$ is due to $5dnp\ ^1P$, and since the series $5dnp\ ^1P$ goes to the $^2D_{5/2}$ threshold,[4] the prescription in Sec. III C. of Ref. 14 leads us to obtain μ_2, for $6snp\ ^1P$, and μ_5, for $5dnp\ ^1P$, from the plot of $-\nu_S$ vs $\nu_{D5/2}$ [Fig. 8(a)]; we find $\mu_2 \simeq 0.77$, $\mu_5 \simeq 0.5$. Since $5dnp\ ^3D$ and ^3P go to the $^2D_{3/2}$ limit, μ_3 and μ_4 are read from Fig. 8(b), in which these states lie on two clearly vertical lines. We find $\mu_3 \simeq 0.72$, $\mu_4 \simeq 0.65$. Note that the $5dnp\ ^3D$ and ^3P states do not lie on vertical lines in Fig. 8(a).

The hand-sketched curves in Fig. 8 are deliberately oversimplified; the only curved lines are those for $6snp\ ^1P$ perturbed by $5dnp\ ^1P$. The straight lines indicate the other, less strongly interacting channels.

Previous analyses of Ca and Sr[3,9] $msnp$ series have shown clear energy dependences for the $msnp$ channels. Figure 9 shows similarly that the $6snp\ ^3P$ channel (open circles) has an energy-dependent eigendefect with $d\mu_1/dE \sim 0.3$. (The energy E is normalized to $I_S = 42\,034.9$ and measured from I_S positively towards lower energy.) Moreover, from the data

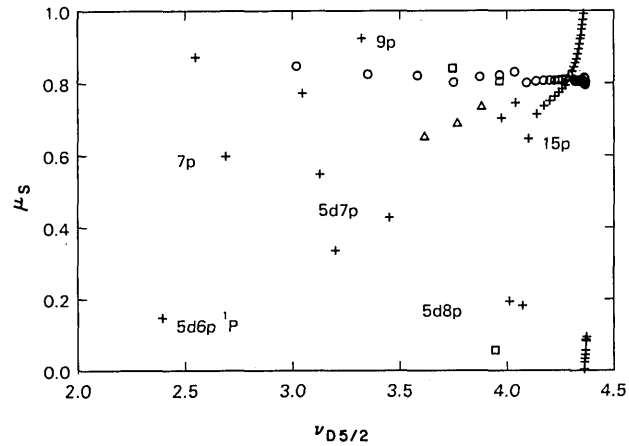

FIG. 9. Lu-Fano plot of odd-parity, $J = 1$ states of Ba without folding $\nu_{D5/2}$ onto the unit square. (symbols as in Fig. 8.)

TABLE X. Interaction angles used to generate V matrix and which couple an $\bar{\alpha}$ channel to an α channel.

$\bar{\alpha}$ \ α	$\alpha=1$	2	3	4	5
1		Θ_1	Θ_2	$\underline{\Theta_3}$	Θ_4
2			$\underline{\Theta_5}$	$\underline{\Theta_6}$	$\underline{\Theta_7}$
3				Θ_8	Θ_9
4					Θ_{10}
5					

on $5d6p$, $7p$ and $8p$ ^3D and ^3P, there is a suggestion that these channels have energy-dependent μ_α as well. The actual MQDT parameters used to fit the data are obtained by a least-squares procedure,[14] starting with values obtained as described above.

The $V_{\bar{\alpha}\alpha}$ matrix, describing mainly configuration interactions, will be generated, following Ref. 23, by successive rotations. The labelling of the rotation angles is shown in Table X. The underlined angles are the only ones required for the five channel fit. Starting values for the angles are best obtained by trial-and-error, which leads eventually to a "feel" for their size. The magnitude of an avoided crossing on a hand-sketched Lu-Fano diagram depends not only on the angles Θ_j, but also on the difference of the relevant eigendefects μ_α.

Of the four angles, Θ_7 is by far the most important; it couples $\bar{\alpha}=2$ with $\alpha=5$, i.e, sp ^1P with "dp" ^1P. Recall that the $\bar{\alpha}$ channels have pure configurations, whereas the α channels have mixed configuration. Hence the labels sp and "dp". Moreover, because of the strong spin-orbit coupling of the $5dnp$ perturbers, a nonzero Θ_7 produces perturbations of $6snp$ ^1P by $5dnp$ ^3D and ^3P as well. *It is found that a suitable choice of Θ_7 explains all of the qualitative features of the perturbed ^1P spectrum.*

However, in order to obtain a really satisfactory, five-channel fit, two further considerations are necessary. The first involves the region around $6s14p$ *and* $6s15p$ ^1P, the second involves changes in shape of the $6snp$ ^1P curve in successive cycles of $\nu_{D5/2}$.

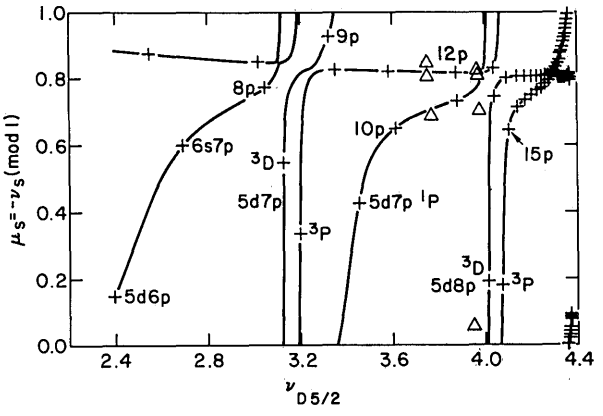

FIG. 10. Five-channel MQDT fit to odd-parity, $J=1$ states of Ba using parameters of Table XI. The data points marked by + are the states which are fit, and the points marked by Δ are not fit.

The $6s14p$ ^1P state occurs near the sudden perturbation of the $6snp$ ^1P channel caused by coupling to the $5dnp$ ^3D channel at $5d8p$. (See Fig. 10 in connection with the following discussion.) If we assume the α channels to be strictly LS coupled, the perburbation of $6snp$ ^1P by $5dnp$ ^3D is fixed by the combination of U^0, the $^2D_{3/2,5/2}$ splitting, and our choice of Θ_7. The resulting fit to $6s14p$ ^1P is inadequate. It is not possible to simultaneously fit $5d8p$ ^3D, the overall shape of the ^1P defects (i.e., Θ_7), *and* fit $14p$ ^1P unless sp ^1P is coupled *directly* to "dp" ^3D, i.e., by a nonzero Θ_5. That is, the set of close-coupling, α channels cannot be exactly LS coupled. A similar deviation from precise LS coupling of the α channels was found in Ref. 3 when describing $^1D_2$ and $^3D_2$ states in Sr. It was also found in describing the even-parity $^1S_0$ states of Ba in Ref. 20. In refining the fit we find that sp ^1P is also weakly coupled to "dp" ^3P *via* Θ_6. There is a small triplet-triplet configuration interaction as well, represented by Θ_3.

The second consideration mentioned above involves the changing shape of the MQDT curve giving the ^1P defects as $\nu_{D5/2}$ goes through two and one-half cycles. This shape, the most striking feature of the $^1P_1^0$ spectrum, is different near $6s15p$ ^1P, $6s10p$ ^1P and $6s7p$ ^1P. In particular, a value of Θ_7 (sp ^1P – "dp" ^1P configuration interaction) which accurately describes the region above $15p$ ^1P, (where there is extensive data) misses $6s7p$ ^1P by hundreds of wave numbers even though lower-lying states (including $5d6p$ ^1P) are well fit. There are similar, but smaller, difficulties in fitting both the $15p$ ^1P and $10p$ ^1P regions with a constant Θ_7. What the data shows is that the ^1P curve becomes "sharper", less flattened, at higher energies (see Fig. 10). That is, *the configuration interaction between sp ^1P and dp ^1P slowly decreases as energy increases.* An energy-dependent angle (as described in Ref. 23) not only allows a vast improvement in MQDT fit to the data but, as will be shown in Ref. 24, describes important features of the autoionizing spectrum as well. *This is the first case where energy dependence has been found in the MQDT angles.* We will comment on the physical significance of this circumstance in Sec. V.

The best fit of a five channel treatment to the data is shown in Fig. 10, using parameters listed in Table XI. The data points labelled Δ are those purposely omitted from the five channel fit, since they involve the $5d4f$ configuration. The four lowest energy states of Table IV were not used in the fit, since MQDT does not do well with the lowest states; likewise, the ten highest states of Table IV were omitted. The goodness of the fit may be described as follows. The average error of the calculated states is less than 10^{-3} cm^{-1}. The rms error is 0.58 cm^{-1}. The least-squares fit of the energies was made using a weight for each state proportional to $(\nu_S)^3$. This is equivalent to a least-squares fit to the quantum defects with equal weights.

Eight-channel treatment

The three $J=1$ channels associated with the $5dnf$ configurations will now be added. The labelling of the eight channels is given in Table XII. We group the collision channels by core state, and so the $i=5$ collision channel in this eight-channel description is different from the $i=5$ collision channel of Table IX.

The angles which generate the $V_{\bar{\alpha}\alpha}$ matrix of the eight-channel treatment are shown in Table XIII, with those that

TABLE XI. Five-channel MQDT parameters for Ba $J = 1$, odd.

α	=	1	2	3	4	5
μ_α	=	0.808 9(06)[a]	0.791 4(15)	0.702 7(11)	0.699 5(22)	0.504 9(13)
$d\mu_\alpha/dE$	=	0.270 1(31)	0.198 (11)	0.303 0(53)	0.071 (11)	−0.293 6(46)
		$(2/3)^{1/2}$	$-(1/3)^{1/2}$	0	0	0
		$(1/3)^{1/2}$	$(2/3)^{1/2}$	0	0	0
$U^0_{i\alpha}$		0	0	$(1/2)^{1/2}$	$-(1/6)^{1/2}$	$(1/3)^{1/2}$
		0	0	$2(1/10)^{1/2}$	$4(1/30)^{1/2}$	$-(1/15)^{1/2}$
		0	0	$-(1/10)^{1/2}$	$3(1/30)^{1/2}$	$3(1/15)^{1/2}$

$\Theta_3 = 0.214\ 5(65)$	couples	$sp\ ^3P$ to "dp" ^3P
$\Theta_5 = 0.356\ 7(75)$	couples	$sp\ ^1P$ to "dp" ^3D
$\Theta_6 = 0.173\ (12)$	couples	$sp\ ^1P$ to "dp" ^3P
$\Theta_7 = 0.571\ 4(31)$	couples	$sp\ ^1P$ to "dp" ^1P
$d\Theta_7/dE = 0.741\ (16)$	energy-dependent coupling[b]	

[a]Probable error in last two digits shown in parentheses.
[b]Since Θ_7 depends on energy, so does $V_{\bar{\alpha}\alpha}$, and we cannot usefully display $V_{\bar{\alpha}\alpha}$ here. See Ref. 23 for the generation of $V_{\bar{\alpha}\alpha}$ from successive rotations.

TABLE XII. MQDT labels for eight-channel fit to Ba $J = 1$, odd.

i, $\bar{\alpha}$	=	1	2	3	4	5	6	7	8
$\lvert i\rangle$	=	$[^2S_{1/2}]p_{1/2}$	$[^2S_{1/2}]p_{3/2}$	$[^2D_{3/2}]p_{1/2}$	$[^2D_{3/2}]p_{3/2}$	$[^2D_{3/2}]f_{5/2}$	$[^2D_{5/2}]p_{3/2}$	$[^2D_{5/2}]f_{5/2}$	$[^2D_{5/2}]f_{7/2}$
I_i	=	42 034.90	42 034.90	46 908.99	46 908.99	46 908.99	47 709.96	47 709.96	47 709.96
$\lvert\bar{\alpha}\rangle$	=	$6snp\ ^3P$	$6snp\ ^1P$	$5dnp\ ^3D$	$5dnp\ ^3P$	$5dnp\ ^1P$	$5ndf\ ^3D$	$5dnf\ ^3P$	$5dnf\ ^1P$

TABLE XIII. Interaction angles in eight-channel case.

		"sp"		"dp"				"df"	
	α=	1	2	3	4	5	6	7	8
	$\bar{\alpha}$								
sp	1		Θ_1	Θ_2	$\underline{\Theta_3}$	Θ_4	Θ_5	$\underline{\Theta_6}$	$\underline{\Theta_7}$
	2			$\underline{\Theta_8}$	$\underline{\Theta_9}$	$\underline{\Theta_{10}}$	Θ_{11}	Θ_{12}	$\underline{\Theta_{13}}$

are nonzero underlined. Note that the angle labels for the same configuration interaction are different in the five-channel and eight-channel fits; i.e., the important configuration interaction $sp\ ^1P$-$dp\ ^1P$ is represented by Θ_7 and Θ_{10}, respectively.

Which elements of the V matrix should we expect to describe the interactions between $6snp$ and $5dnf$? In other words, how do we choose which angles Θ_i should be nonzero? By analogy with the case of the dp perturbers, we expect $6snp\ ^1P$-$5dnf\ ^1P$ to be the most important coupling, so Θ_{13} will be nonzero. This reflects, again, the fact that singlet-singlet configuration interactions are larger than triplet-triplet.

Given the U^0 matrix, a finite value of Θ_{13} can produce avoided crossings near $6s11p\ ^1P$ and $6s13p\ ^1P$, and hence can fit those states (see Fig. 11). However, keeping the sp-dp angles fixed by the five-channel fit, Θ_{13} does not describe the interactions between the two pairs of states remaining. These are the pair at 49 893.48 and 39 916.35 cm^{-1}, and the pair at 40 732.01 and 40 736.81 cm^{-1}. These pairs are primarily admixtures of $6snp\ ^3P$ and $5d4f$; such admixtures are produced by angles Θ_5, Θ_6, and Θ_7 (see Table XIII). In fact we find that only Θ_6 and Θ_7 are required to give a good fit to the observed energies.

From the Ba $J = 1$, odd-autoionizing spectra,[4] we know that the quantum defects of the two $5dnf$ series built on $^2D_{5/2}$ are very nearly the same, whereas the third series goes to $^2D_{3/2}$ and always lies lower in energy for given n. The perturbers which we assign to the $5d4f$ configuration are at 39 893.48, 40 662.86 and 40 736.2 cm^{-1}. The state at 39 893.48 cm^{-1} has a $^2D_{3/2}$ defect of 0.045, whereas the states at 40 662.86 and 40 736.2 cm^{-1} have $^2D_{5/2}$ defects of 0.054 and 0.034, respectively. As initial values of μ_6, μ_7, μ_8 we will therefore use 0.045, 0.054, and 0.034.

The final fit is shown in Fig. 11, and it corresponds to the parameters of Table XIV. The average error in fitting all states except the four lowest is -0.02 cm^{-1}, and the rms error is 0.41 cm^{-1}. The eight-channel fit is quite good for all except the four lowest states of Table IV. However, since there is so little known of the df channels from bound-state data, a more

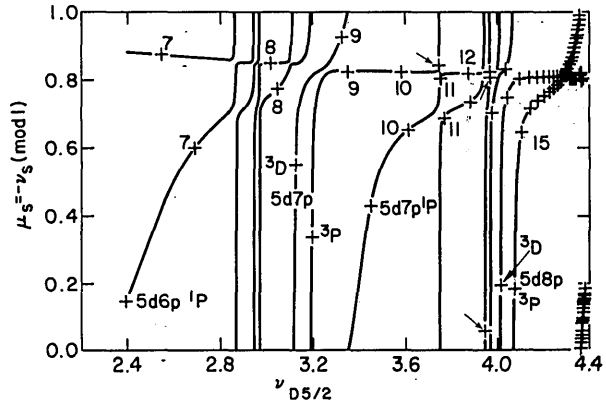

FIG. 11. Eight-channel MQDT fit to odd-parity, $J = 1$ states of Ba using parameters of Table XIV.

TABLE XIV. Eight-channel MQDT parameters for Ba $J = 1$, odd.

α	=	1	2	3	4	5	6	7	8
μ_α	=	0.808 8[a]	0.785 0	0.705 4	0.703 4	0.503 7	0.015 3	0.048 4	0.059 3
$d\mu_\alpha/dE$	=	0.271 5	0.274 9	0.260 1	0.051 7	−0.305 6	0	0	0
		$(2/3)^{1/2}$	$-(1/3)^{1/2}$	0	0	0	0	0	0
		$(1/3)^{1/2}$	$(2/3)^{1/2}$	0	0	0	0	0	0
		0	0	$(1/2)^{1/2}$	$-(1/6)^{1/2}$	$(1/3)^{1/2}$	0	0	0
$U^0_{i\alpha}$	=	0	0	$2(1/10)^{1/2}$	$4(1/30)^{1/2}$	$-(1/15)^{1/2}$	0	0	0
		0	0	0	0	0	$(2/5)^{1/2}$	$-(1/5)^{1/2}$	$(2/5)^{1/2}$
		0	0	$-(1/10)^{1/2}$	$3(1/30)^{1/2}$	$3(1/15)^{1/2}$	0	0	0
		0	0	0	0	0	$4(1/35)^{1/2}$	$3(2/35)^{1/2}$	$-(1/35)^{1/2}$
		0	0	0	0	0	$-(1/7)^{1/2}$	$(2/7)^{1/2}$	$2(1/7)^{1/2}$

$\Theta_3 = 0.2218$	couples	$sp\ ^3P$ to "dp" ^3P
$\Theta_6 = -0.0101$	couples	$sp\ ^3P$ to "df" ^3P
$\Theta_7 = 0.0588$	couples	$sp\ ^3P$ to "df" ^1P
$\Theta_8 = 0.3824$	couples	$sp\ ^1P$ to "dp" ^3D
$\Theta_9 = 0.2013$	couples	$sp\ ^1P$ to "dp" ^3P
$\Theta_{10} = 0.5766$	couples	$sp\ ^1P$ to "dp" ^1P
$\Theta_{13} = 0.1347$	couples	$sp\ ^1P$ to "df" ^1P
$d\Theta_{10}/dE = 0.765\ 6$	energy-dependent coupling	

[a]Probable errors are comparable to those in Table XI.

TABLE XV. Fractional admixtures into heavily mixed states $(Z_{\bar{\alpha}})^2$.

Energy		sp			dp	
$\bar{\alpha}\rightarrow$	Label	^3P	^1P	^3D	^3P	^1P
28 554.257	$5d6p\ ^1P$	0.003	0.496	0.107	0.021	0.349
32 547.076	$6s7p\ ^1P$	0.000	0.715	0.014	0.003	0.240
35 892.52	$6s8p\ ^1P$	0.007	0.802	0.023	0.001	0.160
36 495.62	$5d7p\ ^3D$	0.001	0.079	0.855	0.036	0.066
36 989.98	$5d7p\ ^3P$	0.021	0.024	0.016	0.928	0.016
37 775.28	$6s9p\ ^1P$	0.001	0.632	0.089	0.016	0.271
38 500.29	$5d7p\ ^1P$	0.000	0.549	0.043	0.002	0.388
39 311.95	$6s10p\ ^1P$	0.000	0.918	0.002	0.000	0.077
40 893.76	$5d8p\ ^3D$	0.000	0.106	0.764	0.021	0.086
41 097.2	$5d8p\ ^3P$	0.054	0.301	0.000	0.554	0.068

reliable description of df channels will have to await analysis of the odd-parity, $J = 1$ autoionizing spectrum.[24] Note how much more important the ^1P configurational mixing (Θ_{13}) is than the ^3P mixing (Θ_6) in the sp-df interaction.

Note also in Fig. 11 that the df channels show up as "false-channels" near $\nu_{D5/2} \cong 2.9$. This is the problem of terminating series in MQDT at the lower end, a problem discussed in Ref. 14 for Ca. Fortunately, these "false-channels" occur at an energy region that does not impair the description of the real states.

D. Wave functions and oscillator strengths

We can use the fitting parameters of Table XIV and the procedures of Refs. 3 and 23 to calculate the fractional admixture of pure-configuration basis functions into the actual, observed states.[27] In Tables XV and XVI we show those admixtures for a number of states of interest. In particular, we use the results of the fit to determine the best labels for each state.

The admixtures of pure-configuration, $\bar{\alpha}$-basis states into the most heavily mixed states are shown in Table XV. Note that each state labelled with a particular designation is the

TABLE XVI. Fractional admixtures into states perturbed by $5d4f$.

Energy	Label	sp ($\bar{\alpha} \rightarrow {}^3P$	^1P)	df $\left(i \rightarrow \frac{3\ 5}{2\ 2}\right.$	$\frac{5\ 5}{2\ 2}$	$\left.\frac{5\ 7}{2\ 2}\right)$
39 893.48	$5d4f\ \frac{3\ 5}{2\ 2}$	0.424	0.045	0.521	0.003	0.003
39 916.35	$6s11p\ ^3P$	0.568	0.068	0.357	0.001	0.001
40 662.86	$5d4f\ \frac{5\ 7}{2\ 2}$	0.007	0.077	0.002	0.097	0.789
40 732.01	$6s13p\ ^3P$	0.802	0.011	0.002	0.178	0.002
40 736.81	$5d4f\ \frac{5\ 5}{2\ 2}$	0.168	0.361	0.004	0.423	0.003

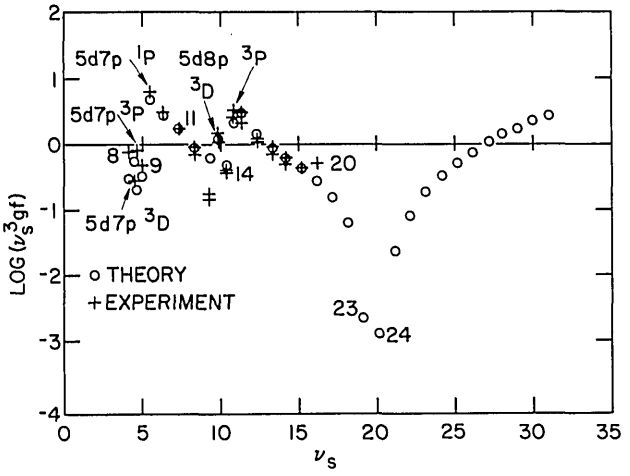

FIG. 12. Oscillator strengths of $^1P_1^0$ states of Ba. Experimentally determined values as given in Ref. 28 are represented by + symbols. Our MQDT determined theoretical values are represented by the O symbols.

state with the *largest* admixture of that pure-configuration, $\bar{\alpha}$-basis function. This labelling is consistent with that of previous authors. It is not necessarily the case, of course, that a state labelled with a particular perturbing configuration and designation is *primarily* that configuration; for example, the state labelled $5d6p\ ^1P$ contains only 35% of $5dnp\ ^1P$ character.

The df perturbers are shown in Table XVI. Here we have used a hybrid labelling scheme, because the bound df perturbers are more nearly pure jj-coupled states than they are pure LS-coupled or jK-coupled states. The $6snp$ states affected by $5d4f$ pertubers should still be reasonably well described by LS coupling. The states at 39 893.48 and 39 916.35 cm^{-1} are strongly mixed, with the labels simply reflecting "majority rule". The lower of these two is our assignment to $5d(^2D_{3/2})4f_{5/2}$, and is the "missing" lowest member of the series called E in Ref. 4. Similarly, the other "missing" state is the state we found at 40 662.86 cm^{-1} and labelled $(^2D_{5/2})$-$4f_{7/2}$. Note that Garton and Tomkins used jK notation for $5dnf$, whereas we are using jj notation; the $jj = 3/2, 5/2$ channel is the same as their $jK = (3/2)(3/2)$ channel, but the other two channels transform with linear combinations under the change from jj to jK coupling.

It is also of interest to see how the MQDT analysis describes the oscillator strengths of the Ba $J = 1$, odd states. The known behavior of the oscillator strengths is quite complex,[28] and deviates dramatically from a simple ν_S^{-3} behavior. To describe oscillator strengths, following Ref. 23, we introduce three additional parameters, called "eigenoscillator strengths", $D_{\bar{\alpha}}$, for the three $\bar{\alpha}$ channels which are rigorously $^1P_1$ and are therefore the only $\bar{\alpha}$ channels connected to the ground-state $^1S_0$ by a one-photon transition. Figure 12 shows the theoretical oscillator strengths compared to those of Miles and Wiese and Parkinson *et al.*[28] The starting values of D_2, D_5, D_8 were chosen to fit $6s10p$, $11p$, $12p\ ^1P$ using Miles and Wiese's experimental data. The resulting $D_{\bar{\alpha}}$ produced the Fano-minimum at $n = 23$ instead of $n = 24$ (see discussion in Sec. II). A small adjustment in D_5, well within what is allowed by the uncertainties in experimental values, moves the minimum to $n = 24$, as shown in Fig. 12. The three values which yield Fig. 12 are $D_2 = 0.004\,243$, $D_5 = -0.003\,946$ and $D_8 = -0.000\,295$. The *relative* signs of the $D_{\bar{\alpha}}$ are uniquely determined.

The behavior of the oscillator strength is due to the fact that each of the $5dnl$ states perturbs 6^1P and imparts some oscillator strength to the series; the $5d8p\ ^1P$ state has its oscillator strength diluted into all the $6snp\ ^1P$ states above $n = 24$ as well as into the first 400 cm^{-1} of the continuum.[24] It is clear from Fig. 12 that the MQDT analysis does a good job describing the complex variation of oscillator strengths for all states which are well fit in energy. The lowest states, $6s6p\ ^{1,3}P$, $5d6p\ ^{1,3}P$ and ^3D are not well fit by MQDT, either in energy or oscillator strengths; this is not surprising, since the MQDT model is really applicable only to electrons "well removed" from the core.

There is one final comparison which can be made with experimental oscillator strengths. Carlsten and McIlrath[29] measured the absolute absorption cross section of Ba at 2379 Å, the peak of the $5d8p\ ^1P$ resonance, which is right on the ionization limit. Their measurement, which used a hook determination of vapor density *via* the 3072 Å line ($6s^2\ ^1S_0$-$6s7p\ ^1P$), can be expected to be much better than previous determinations. Their value for the cross section at 42 034 cm^{-1} is $(50 \pm 8) \times 10^{-18}$ cm^2. Expressed in terms of df/dE, the oscillator strength density in the continuum, the value is $df/dE = (0.46 \pm 0.07)$ $(eV)^{-1}$. In converting units we have used the relation $\sigma(E) = 1.098 \times 10^{-16}$ cm^2 eV (df/dE), due to Fano and Cooper.[30] Using the parameters of Table XIV, the $D_{\bar{\alpha}}$ given above, and the formulas of Ref. 23, the eight-channel MQDT treatment predicts $df/dE = 0.51$ eV^{-1} at 42 034 cm^{-1} ($\sigma_{MQDT} = 56 \times 10^{-18}$ cm^2). This value agrees with Ref. 29 to within the standard deviation of Carlsten and McIlrath's measurements.

The success and utility of MQDT is to be judged by how well it reproduces energies and oscillator strengths on both sides of the ionization limit. Clearly the MQDT description of the Ba, $J = 1$, odd spectrum is very good below and at I_S; the comparison between experiment and theory above I_S will be made in Ref. 24.

E. Other states in barium

Extensive new data on series of states other than $J = 1$, odd parity were presented in Sec. III. Here we analyze and discuss this in terms of MQDT.

Each $6snp\ ^3P^0$ term is split by spin-orbit effects into $J = 0$, 1 and 2 states. Transitions from $6s7s\ ^3S_1$ to all three states are allowed by the $\Delta J = 0, \pm 1$ selection rule. In general our spectra taken with excitation from $6s7s\ ^3S_1$ showed resolved $^1P_1^0$, $^3P_1^0$, and $^3P_2^0$ states for $n \leq 20$. For $n = 21$ and 22, $^3P_2^0$ was not resolved from $^1P_1^0$, and for $n \geq 23$, $^3P_1^0$ was not resolved from $^3P_2^0$.

The lowest n reached in excitation from $^3S_1$ was $n = 11$. Our spectral scans showed several peaks and shoulders on other peaks which were potentially due to $J = 0$ states. We applied the procedure discussed in Sec. III in which laser polarization and detuning are used to identify $J = 0$ states. Of the peaks we checked, only two were positively identified

TABLE XVII. Two-channel MQDT parameters for Ba $^3P_2^0$.

α	=	1	2
μ_α	=	0.780 7(3)[a]	0.383 05(2)
$d\mu_\alpha/dE$	=	0.25(1)	0
U_{21}	=	0.033 36(7)	
Ionization limit I_S	=	42 034.88(1)	I_d = 46 908.99

[a] Probable error in last digit shown in parentheses.

as having $J = 0$. These are listed in Table III. The state is labelled $6s16p\ ^3P_0^0$ appeared as a partially resolved peak below the $6s16p\ ^3P_1^0$ state. The other state is labelled $5d8p\ ^3P_0^0$ in Table III because it lies only ~13 cm^{-1} below $5d8p\ ^3P_1^0$. The corresponding splittings for $5d6p$ and $5d7p\ ^3P$ are ~62 cm^{-1} and 82 cm^{-1} respectively.[7]

Careful attempts to isolate and identify $6snp\ ^3P_0^0$ states with n = 11, 12, 13, 14, 15, and 17 were unsuccessful. Peaks at 39 902.44 and 40 392.42 cm^{-1} might be due to $6s11p$ and $12p\ ^3P_0^0$, but we could not verify them. No peaks which might be due to $6s13p$ or $14p\ ^3P_0^0$ were seen. This may be due to the shift of $6s13p$ and $14p\ ^3P_1^0$ to lower energy due to configuration interaction so that they overlap and obscure the corresponding $^3P_0^0$ states. The $6s15p$ and $17p\ ^3P_1^0$ peaks showed unresolved, low-energy shoulders. Detuning and polarization studies showed that the low-energy shoulder at $6s15p\ ^3P_1^0$ appeared in the coherent (shifted) peak only for perpendicular polarizations of ν_2 and ν_3, in support of the identification of this shoulder as due $6s15p\ ^3P_0^0$. We estimate this shoulder to occur at 41 159.3 cm^{-1}. Similar studies on the $6s17p\ ^3P_1^0$ shoulder were inconclusive. For higher n, our experimental resolution was insufficient to reveal further $^3P_0^0$ peaks or shoulders.

The $6snp\ ^3P_2^0$ states were easily resolved except for n = 21 and 22 where they overlapped the $^1P_1^0$ states. The $J = 2$, odd spectrum has a single perturber at 41 759.93 cm^{-1}, marked by P in Fig. 3. The data in Table V, excluding the lowest energy state, were fit by the two-channel MQDT parametrization given in Table XVII, in which I_S was also fit. From these parameters, values for n = 21 and 22 were calculated. Comparison of these calculated values with the measured $6s21p$ and $6s22p\ ^1P_1^0$ energies (Table IV) show that they are very close, consistent with our inability to experimentally resolve the $^3P_2^0$ states. Our MQDT fit to the $^3P_2^0$ states has an average error of 0.022 cm^{-1} and an rms error of 0.046 cm^{-1}.

For the $6s16p$ state, where $^1P_1^0$, $^3P_0^0$, $^3P_1^0$, and $^3P_2^0$ were all identified, we find the interval ratio $(^3P_2^0 - {}^3P_1^0)/(^3P_1^0 - {}^3P_0^0) = 2.30$. The intervals together with the separation of $^1P_1^0$ and $^3P_1^0$ result in an estimate of $a^2 \sim 3 \times 10^{-2}$ for $^1P_1^0$ and $^3P_1^0$ mixing for these states.

TABLE XVIII. One-channel QDT parameters for Ba $^1G_4$.

μ	=	0.058(2)[a]
$d\mu/dE$	=	−0.1(1)
I_S	=	42 034.93(2)

[a] Probable error in last digit shown in parentheses.

Another state which appears to have $J = 2$ was labelled as follows. This state did not appear in absorption (hence $J \neq 1$), but was seen as a strong peak in excitation from $6s7s\ ^3S_1$. Detuning and polarization studies showed it to appear in both perpendicular and parallel polarizations of ν_2 and ν_3, eliminating a $J = 0$ identification. Hence it has $J = 2$. It has an energy of 39 898.56 ± 0.19 cm^{-1}, ~5 cm^{-1} above a $5d4f\ J = 1$ state (Table IV). Hence we tentatively label it $5d4f\ J = 2$.

The other $J = 2$ states we observed in excitation from $6s7s\ ^3S_1$ are the $6snf\ ^3F_2^0$ states listed in Table VI. These states have been seen in absorption from the $6s5d\ ^3D_1$ by Carlsten *et al.*[31] Our measurements agree with theirs to better than 1 cm^{-1} (with the exception of $6s11f$). The $6s20f\ ^3F_2$ is slightly perturbed to lower energy. The source of perturbation is the state (P) mentioned in the previous paragraph that also perturbs the $^3P_2^0$ series. This state has a stronger effect on the $^3P_2^0$ series than on $^3F_2^0$. It is the only perturber of $^3P_2^0$ we observed and it lies above $5d8p\ ^3P_1^0$. Thus our best guess for a label for this perturber is $5d8p\ ^3P_2^0$.

The last series we identified in Ba is $6sng\ ^1G_4$. Data for this series are presented in Table VII. A single channel fit to the first 42 of these states is given in Table XVIII where I_S was allowed to float. This fit has an average error of less than 10^{-3} cm^{-1} and an rms error of 0.07 cm^{-1}.

V. DISCUSSION

We have described the experimental method used to observe bound triplets and other "hard-to-find" states in Ca, Sr, and Ba, presented MQDT analyses of the data, and given tables of our newly identified states with classification labels based on the MQDT analyses. We will now examine these results, comparing the MQDT parameters for Ca, Sr, and Ba, and commenting upon the observed differences in the singlet and triplet spectra.

Our first comment concerns the great similarities among Ca, Sr, and Ba which emerge from the MQDT analyses of the $^1P_1^0$ and $^3P_1^0$ configuration interactions in these different atoms. In Table XIX we present separated groups of two-channel MQDT parameters for $^1P_1^0$ and $^3P_1^0$ states. For Ca and Sr,

TABLE XIX. Comparison of two-channel MQDT parameters.

		Ca	Sr	Ba
$^1P_1^0$	μ_1[a]	0.99	0.93	0.83
	μ_2[b]	0.57	0.49	0.43
	$\Delta = \mu_1 - \mu_2$	0.42	0.44	0.40
	$\bar{\mu} = (\mu_1 + \mu_2)/2$	0.78	0.71	0.63
	U_{21}	0.56	0.58	0.58
$^3P_1^0$	μ_1[a]	0.03	0.94	0.91[c]
	μ_2[b]	0.84	0.81	0.73[c]
	Δ	0.19	0.13	0.18
	$\bar{\mu}$	0.94	0.88	0.82
	U_{21}	0.31	0.41	0.21[d]

[a] μ_1 refers to the $msnp$ channel with m = 4, 5 and 6 for Ca, Sr and Ba respectively.
[b] μ_2 refers to the $(m-1)dnp$ channel.
[c] These values are extracted from Table XI.
[d] This value is generated from the rotation angle Θ_3 in Table XI.

these parameters are taken from Table VIII with allowance for energy dependence so that the value of μ_1 corresponds to the energy of the state labelled as the perturber ($3d4p$ or $4d5p$ for Ca and Sr, respectively). For the $^1P_1^0$ case in Ba, the two-channel parameters result from an approximate fit to the four states labelled $5d6p$, $6s7p$, $6s8p$, and $6s9p$ $^1P_1^0$ (this limited choice of states will be justified shortly). For the $^3P_1^0$ case in Ba, the parameters are extracted from Table XI (five-channel MQDT fit) by correlating μ_1 and μ_2 with $\alpha = 1$ and 4, and by taking $U_{21} = \sin\Theta_3$.

The most striking observation is that the Lu-Fano plots for Ca and Sr $^1P_1^0$, given in Figs. 7(a) and 7(b), are almost exactly the same if we displace one along the upper-left-to-lower-right diagonal within the unit square to overlap the other. This reflects the fact that the *shape* of the two-channel theoretical curves *depends only on the difference* $\Delta = \mu_1 - \mu_2$ *and on* U_{21}. Displacing the curves within the unit square along the upper-left-to-lower-right diagonal corresponds to changing μ_1 and μ_2 by the same amount, thereby keeping Δ constant. This may be shown analytically from the fundamental determinental equations[32]

$$\det|U_{i\alpha}\sin\pi(\nu_i + \mu_\alpha)| = 0. \quad (1)$$

For a two-channel problem, this may be expressed as[33]

$$[\tan\pi(\nu_1 + \bar{\mu}) + \tan\pi(\Delta/2)\cos2\Theta][\tan\pi(\nu_2 + \bar{\mu}) - \tan\pi(\Delta/2) \times \cos2\Theta] = \tan^2\pi(\Delta/2)\sin^2 2\Theta, \quad (2)$$

where $\bar{\mu} = (\mu_1 + \mu_2)/2$ and $U_{21} = \sin\Theta$. Equation (2) shows that changing $\bar{\mu}$ while keeping Δ constant does not change the functional dependence of $(\nu_1 + \bar{\mu})$ on $(\nu_2 + \bar{\mu})$ but simply displaces a plot of ν_1 vs ν_2 along the diagonal, $\nu_1 = \nu_2$. The significance of this possibility to superpose the $^1P_1^0$ curves for Ca and Sr is that the interaction *between channels*, described by Δ and U_{21}, is nearly the same for the two atoms. The interaction of the excited electron with the tight ionic core changes from Ca to Sr, changing the value of $\bar{\mu}$.

Next, we needed to get two-channel parameters for Ba in order to compare it to Ca and Sr. Ba has three bound members of the $5dnp$ $^1P_1^0$ channel, and the angle, Θ_7, is energy dependent. For consistency, we chose to find parameters in the vicinity of the lowest $^1P_1^0$ perturber, $5d6p$, since in Ca and Sr only the lowest perturber of the $(m-1)dnp$ channel is bound. Thus we chose to make a two-channel fit to the four states which lay near the branch of the curve which contains $5d6p$. Our fit to these four states results in the parameters given in Table XIX. One sees immediately the similarity to Ca and Sr when comparing Δ and U_{21}. Thus, when expressed in terms of the MQDT set of atomic parameters, *the configuration interaction is basically the same for the msnp and* $(m-1)dnp$ *channels for all three atoms.* This is a testimony to the utility of MQDT in exhibiting the underlying and essential features of two-electron spectra.

The similarity of the $^3P_1^0$ spectra is less dramatic. The curves in Fig. 7(c) and 7(d) for Ca and Sr look quite similar and show much less curvature than the corresponding singlet curves. The parameters in Table XIX show a greater variation for triplets than they do for singlets.

Our second comment is concerned with the smaller triplet configuration interaction as compared to the singlets. In every case where we have observed both singlets and triplets of the same J, L, and parity (in both this paper and in Refs. 3 and 14), the effects of configuration interaction on the singlets is much greater than its effect on the triplets. Shore and Menzel[34] express the configuration-interaction matrix element M for an $sp - dp$ interaction as $M = R^2 + (-1)^S R^1$, where R^2 and R^1 are generalized Slater integrals and S is the total spin. Previous workers[35] have found that for particular configurations of particular atoms, R^2 and R^1 have the same sign and comparable magnitudes, leading to smaller configuration interaction for triplets than for singlets. Our results lead us to suggest that (i) there exist analogous radial integrals R^2 and R^1, which characterize entire channels and are normalized per unit energy, thus being essentially independent of the running radial quantum number, (ii) the configuration interaction between channels is proportional to $R^2 + (-1)^S R^1$, and (iii) R^2 and R^1 have the same sign and comparable magnitude.

Another subject which deserves comment is the energy-dependent angle found necessary to describe the Ba $^1P_1^0$ spectrum; intimately connected with that result is the unusual energy dependence found for μ_5. Since this is the first case in which these dependences have been found, it is premature to give a "full" explanation. One thing seems clear; the unusual energy dependence of the "dp" ^1P eigendefect μ_5 is not a separate phenomenon from the energy-dependent angle. In attempting to fit the Ba $J = 1$, odd spectrum *without* using energy dependent angles, least-squares fits to the μ_α and $d\mu_\alpha/dE$ did not even product clear cut *signs* for the energy dependence in μ_3, μ_4, and μ_5. Once the energy dependence in the angle describing the sp – "dp" ^1P configuration interaction was invoked, not only was there a dramatic improvement in the fit, but the energy dependences of μ_3 and μ_4 turned out to be "ordinary"—that is positive in our units and of magnitude 0.3 and 0.07, respectively (for the five-channel fit). In contrast μ_5 was found to have an energy dependence of opposite sign.

Very little may be said, after only one case, about the physical cause of the energy-dependent angle. The sign *is* what one would expect; that is, as energy increases and the wave functions of both channels become more extended, the sp – "dp" ^1P configuration interaction decreases.

The magnitude of the angle energy-derivative explains not only the changing "shape" of the bound ^1P defects versus $\nu_{D5/2}$, but accounts also for the variation in linewidth of the first few autoionizing lines of $5dnp$ ^1P character.[24]

With regard to the magnitude of the angles *per se* (not their energy derivatives) we make the following comments. In factoring $U_{i\alpha}$ into $U^0_{i\bar{\alpha}}V_{\bar{\alpha}\alpha}$ we have chosen $U^0_{i\bar{\alpha}}$ to be the matrix transforming from LS to jj coupling in pure configurations; but we might have chosen a different U^0 matrix. Had we done so, the magnitudes of the angles generating $V_{\bar{\alpha}\alpha}$ would have been altered (although the resulting $U_{i\alpha}$ would have been the same). We believe that the choice we have made for $U^0_{i\bar{\alpha}}$ makes good sense, but we note that it is not unique.

Finally, we note that some odd-parity states which we might have expected to see were not identified. In particular, the $5d8p$ $^3D_2^0$ and $5d4f$ $J = 0$ and $J = 2$ states were not identified, although our excitation spectra from the $6s7s$ $^3S_1$ state should show them. Our spectra have many unidentified peaks and it is possible to make guesses as to their identity. Strong

peaks at 40 678.91 ± 0.18, 40 792.94 ± 0.15 and 40 946.20 ± 0.15 cm^{-1} did not appear in absorption or in excitation from $6s7s\ ^1S_0$ so they are almost surely not $J = 1$ states. The sizes of these peaks did not appear to depend on pressure. From their positions relative to identified $J = 1$ perturbers, we make the following *tentative* assignments: $5d4f\ J = 2$, 40 678.91 and 40 792.94 cm^{-1}; and $5d8p\ ^3D^0_2$, 40 946.2 cm^{-1}. There should also be a single $5d4f\ J = 0$ state and one more $5d4f\ J = 2$ state. Their identifications and confirmations of our other tentative labels remain for future spectroscopic studies.

As an historical note, we point out that the first paper[36] to use Lu-Fano plots for graphical analysis of perturbed Rydberg series presented a sketch for the odd-parity $J = 1$ states of Ba. It is interesting to compare Fig. 4 of Ref. 36 to our Fig. 11 and to see how MQDT has been able to deal *quantitatively* with all details of the spectrum.

Future work on the alkaline earth spectra will include (i) a treatment of the odd-parity $J = 1$ autoionizing spectra of Ba up to the ^2D thresholds,[24] and (ii) an analysis of the even-parity $J = 0$, 1 and 2 autoionizing spectra of Ca (Ref. 37) and Ba (Ref. 38).

A recent study of the odd-parity $J = 1$ series of Ba converging on the ^2P thresholds[39] show no evidence that these channels interact with those we have considered in this paper.

ACKNOWLEDGMENTS

We wish to express our appreciation to L. H. Manganaro for his able technical assistance in the experimental aspects of this work. We also thank Dr. J. P. Hermann for his experimental verification of some of the J assignments in Ba. We are grateful to Dr. K. T. Lu and Dr. U. Fano for extensive discussions on the application and interpretation of MQDT. We also acknowledge useful discussions with Dr. M. L. Ginter and Dr. T. J. McIlrath. The U. S. Army Research Office supported this work in part.

[1]C. M. Brown, S. G. Tilford, and M. L. Ginter, "Absorption spectrum of Ca I in the 1580–2090 Å region," J. Opt. Soc. Am., **63**, 1454–1462 (1973).
[2]W. R. S. Garton and K. Codling, "Ultraviolet Extensions of the Arc Spectra of the Alkaline Earths: The Absorption Spectrum of Strontium Vapour," J. Phys. B **1**, 106–113 (1968).
[3]P. Esherick, "Bound, even-parity $J = 0$ and $J = 2$ spectra of Sr," Phys. Rev. A **15**, 1920–1936 (1977).
[4]W. R. S. Garton and F. S. Tomkins, "Ba I Absorption-Line Series at High Resolution," Astrophys. J. **158**, 1219–1230 (1969).
[5]C. E. Moore, *Atomic Energy Levels*, Vol. 1, NBS Circ. No. 467 (U. S. Government Printing Office, Washington, DC, 1949), p. 243.
[6]C. E. Moore, *ibid.* Vol. 2 (1952), p. 190.
[7]C. E. Moore *ibid.* Vol. 3 (1958), p. 132.
[8]U. Fano, "Unified treatment of perturbed series, continuous spectra and collisions," J. Opt. Soc. Am. **65**, 979–987 (1975) and references contained therein.
[9]P. Esherick, J. J. Wynne, and J. A. Armstrong, "Spectroscopy of $^3P^0$ States of Alkaline Earths," Opt. Lett. **1**, 19–21 (1977).
[10]P. Esherick, J. A. Armstrong, R. Dreyfus, and J. J. Wynne, "Miltiphoton Ionization Spectroscopy of High-Lying, Even-Parity States in Calcium," Phys. Rev. Lett. **36**, 1296–1299 (1976).
[11]Recently, many of the $6snp\ ^3P^0_1$ states in Ba, reported here for the first time, have also been seen in absorption by C. M. Brown using photographic detection and by J. A. Armstrong and F. S. Tomkins using photoelectric detection. These workers also observed both the $6s23p$ and $24p\ ^1P^0_1$ states. (private communication.)
[12]D. Popescu, C. B. Collins, B. W. Johnson, and I. Popescu, "Multiphoton excitation and ionization of atomic cesium with a tunable dye laser," Phys. Rev. A **9**, 1182–1187 (1974); K. C. Harvey and B. P. Stoicheff, "Fine Structure of the n^2D Series in Rubidium Near the Ionization Limit," Phys Rev. Lett. **38**, 537–540 (1977); P. Esherick and J. J. Wynne, "High Rydberg States in Alkaline Earth Atoms-I: Multiphoton Spectrosocpy," Comments Atomic Mol. Phys. **7**, 43–52 (1977).
[13]K. H. Kingdon, "A method for the neutralization of electron space charge by positive ionization at very low gas pressures," Phys. Rev. **21**, 408–418 (1923).
[14]J. A. Armstrong, P. Esherick, and J. J. Wynne, "Bound, even-parity $J = 0$ and 2 spectra of Ca: A multichannel quantum defect theory analysis," Phys. Rev. A **15**, 180–196 (1977).
[15]T. W. Hänsch, "Repetitively Pulsed Tunable Dye Laser for High Resolution Spectroscopy," Appl. Opt. **11**, 895–898 (1972).
[16]W. R. S. Garton and K. Codling, "Ultraviolet Extensions of the Arc Spectra of the Alkaline Earths: The Absorption Spectrum of Barium Vapour," Proc. Phys. Soc. Lond. **75**, 87–94 (1960).
[17]U. Fano, "Effects of configuration interaction on intensities and phase shifts," Phys. Rev. **124**, 1866–1878 (1961).
[18]D. Grischkowsky, "Coherent excitation, incoherent excitation, and adiabatic states," Phys. Rev. A **14**, 802–812 (1976).
[19]J. R. Rubbmark, S. A. Borgström, and K. Bockasten, "Absorption Spectroscopy of Laser-Excited Barium," J. Phys. B **10**, 421–432 (1977).
[20]M. Aymar, P. Camus, M. Dieulin, and C. Morillon, "Two-photon spectroscopy of neutral Barium: Observation of the highly excited even levels and theoretical analysis of the $J = 0$ spectrum," Phys. Rev. A (to be published).
[21]M. J. Seaton, "QDT," Comments Atomic Mol. Phys. D **2**, 37–46 (1970); Also "Quantum Defect Theory I. General Formulation," Proc. Phys. Soc. Lond. **88**, 801–814 (1966).
[22]K. T. Lu, "Spectroscopy and collision theory. The Xe absorption spectrum," Phys. Rev. A **4**, 579–596 (1971).
[23]C. M. Lee and K. T. Lu, "Spectroscopy and collision theory. II. The Ar absorption spectrum," Phys. Rev. A **8**, 1241–1257 (1973).
[24]J. A. Armstrong and F. S. Tomkins (unpublished).
[25]K. T. Lu, "On the Interaction Between the $5s$-p and $4d$-p Channels of Sr I," Proc. R. Soc. Lond. A **353**, 431–440 (1977).
[26]For Ca the singlet $4s6p$ to $4s9p$ energies are taken from G. Risberg, "The Spectrum of Atomic Calcium, Ca I, and Extensions to the Analysis of Ca II," Ark. Fys. **37**, 231–249 (1968); the $4s10p$ energy is taken from W. R. S. Garton and K. Codling, "Ultraviolet Extensions of the Arc Spectra of the Alkaline Earths: The Absorption Spectrum of Calcium Vapour," Proc. Phys. Society Lond. **86**, 1067–1075 (1965); and the $4s11p$ and higher n energies are taken from Ref. 1. For Sr the singlet data is taken from Ref. 6 and Ref. 2.
[27]Note that, although we have expressed $d\mu/dE$ in terms of an energy normalized to I_S in Tables VIII, XI, and XIV, the energy derivative used in calculating the normalization integrals and mixing coefficients, following the procedures of Ref. 23, must be expressed in atomic units. This means that the energy derivatives given in our tables must be multiplied by $-2R/I_S$.
[28]B. M. Miles and W. L. Wiese, "Critical Evaluation of Transition Probabilities for Ba I and Ba II," Atomic Data **1**, 1–17 (1969); W. H. Parkinson, E. M. Reeves, and F. S. Tomkins, "Neutral Calcium, Strontium and Barium: Determination of f-values of the Principal Series by the Hook Method," J. Phys. B **9**, 157–165 (1976).
[29]J. L. Carlsten and T. J. McIlrath, "Revised Absolute Absorption Cross section of Ba I at 237.9 nm," J. Phys. B **6**, L284–285 (1973).
[30]U. Fano and J. W. Cooper, "Spectral Distribution of Atomic Oscillator Strength," Rev. Mod. Phys. **40**, 441–507 (1968).
[31]J. L. Carlsten, T. J. McIlrath, and W. H. Parkinson, "Absorption Spectrum of the Laser-Populated ^3D Metastable Levels in Barium," J. Phys. B **8**, 38–51 (1975).
[32]Ref. 14, Eq. (4b).
[33]U. Fano, "Quantum defect theory of l uncoupling in H_2 as an example of channel-interaction treatment," Phys. Rev. A **2**, 353–365 (1970). Our Eq. (2) is a version of his Eq. (34) modified for bound states.
[34]B. W. Shore and D. H. Menzel, *Principles of Atomic Spectra*, (Wiley, New York, 1968), p. 358.
[35]W. C. Martin and J. Sugar, "Perturbation and coupling in the d^9sp configurations of Cu I, Zn II, Ag I, Cd II, and Tl III," J. Opt. Soc. Am.

59, 1266–1280 (1969); W. C. Martin, J. Sugar, and J. L. Tech, "Application of Slater-Condon theory with configuration interaction to the $5d^{10}\,6s6p$, $5d^{9}\,6s^{2}\,6p$, $5d^{10}\,6s7p$, and $5d^{10}\,6s5f$ configurations in Hg I, Tl II, Pb III and Bi IV," Phys. Rev. A 6, 2022–2035 (1972).
[36]K. T. Lu and U. Fano, "Graphic analysis of perturbed Rydberg series," Phys. Rev. A 2, 81–86 (1970).
[37]J. J. Wynne, J. A. Armstrong, and P. Esherick, "Spectroscopy of the Autoionizing, Even-Parity $J = 0$, 1 and 2 States of Ca," Bull Am. Phys. Soc. 22, 64 (1977).
[38]J. J. Wynne and J. P. Hermann, "Spectroscopy of even-parity autoionizing states of Ba," Annual meeting of OSA, San Francisco, California, Oct. 31–Nov. 3, 1978, Paper ThC6, J. Opt. Soc. Am., 68, 1412, (1978).
[39]C. M. Brown and M. L. Ginter, "Absorption spectrum of Ba I between 1770 and 1560 Å," J. Opt. Soc. Am. 68, 817–825 (1978).

Hyperfine structure measurements of high-lying levels of uranium

L. A. Hackel, C. F. Bender, M. A. Johnson, and M. C. Rushford
Lawrence Livemore Laboratory, P. O. Box 5508, Livermore, California 94550
(Received 10 July 1978; revised 3 October 1978)

A technique for precisely measuring hyperfine structure of any level of neutral uranium which can be excited by a single or multistep transition from the ground or a low-lying metastable state has been developed. Numerous spectra were measured and fit to obtain precise hyperfine splitting constants. In particular, measurements on the 31 869-cm^{-1} odd level have determined the following: $J = 6$, magnetic dipole constant $A = -47.2 \pm 0.6$ MHz and electric quadrupole constant $B = 1892 \pm 26$ MHz. Structure of serveral excited states of known configuration were measured including the 15 632-cm^{-1} $f^2d\,^2s\,^2(^5L_7)$ and the 16 930-cm^{-1} $f^3dsp\,(^7K_5)$ levels.

We report on the development of a technique which allows us to accurately measure hyperfine structure (hfs) in uranium for many energy levels below the first ionization limit. In particular, we have resolved with up to 60-MHz resolution and 10-MHz accuracy the hyperfine structure on several transitions between the ground state and 15 000 to 17 000 cm^{-1}, and have determined accurate values for their magnetic dipole (A) and electric quadrupole (B) coupling constants. In addition, we have, for the first time, measured detailed hyperfine structure of a level as high as 32 000 cm^{-1}.

We find in the literature measurements of hyperfine constants for only a single transition in uranium—the 5915-Å resonance line. This line has an unusually large (6 GHZ) hyperfine structure splitting and Gerstenkorn, *et al.*[1] were able to resolve some of the strong $\Delta F = \Delta J$ components as well as one of the weak $\Delta F = 0$ components to deduce A and B constants for both the ground and 16 900-cm^{-1} levels. Subsequently Bohm remeasured the 5915-Å line and obtained values which were significantly different.[2]

Our technique is similar to one discussed earlier[3] and employs an atomic beam of uranium with Doppler bandwidth as narrow as 60 MHz crossed with a combination of pulsed and cw dye lasers. Figure 1 shows a schematic diagram of the experimental setup. The N_2-pumped pulsed dye laser No. 1 with a bandwidth of 30 GHz is used to populate all the hyperfine states of the lower level of interest (not necessary when this level is the ground or a thermally populated metastable state). The stable, precisely tuned cw dye laser No. 2 is then scanned across the hyperfine structure. This laser has a bandwidth of several MHz and thus, becomes our high-resolution probe. Finally, another pulsed dye laser, No. 3, pumps these doubly excited atoms into an autoionizing level where they spontaneously ionize. The ions are filtered through a quadrupole mass spectrometer and detected on a particle multiplier. The ion pulses are gated out with a boxcar averager and then fed to a signal averager which allows us to sum numerous scans across the hyperfine structure. By rapidly dithering the average frequencies of the broadband lasers used to populate and to ionize the hyperfine components being studied, we were able to eliminate the effects of spectral inhomogeneity of these lasers.

At the heart of our system is a precisely tuned cw dye laser (Spectra Physics 580A). A feedback loop is used to lock the fine-tuning etalon bandpass to the laser cavity resonance allowing us to smoothly scan without mode hopping. To obtain a linear scan, a servo locks the laser frequency to an 8-GHz free spectral range (FSR) Fabry Perot etalon which needs to be displaced only $\lambda/2$ for a typical full scan. A 300-MHz FSR Fabry Perot etalon serves to provide frequency markers and indicates that the scans are linear to about 1%.

The hyperfine component positions and intensities can be described with two hyperfine splitting constants,[4] A for the magnetic dipole interaction and B for the electric quadrupole interaction. These constants are extracted from the measured hfs component positions and intensities using standard fitting techniques. Assuming the lower-level constants are known, the upper-level parameters are varied until reasonable positions are obtained for more intense (3–4) components. Intense components are then assigned and the constants which minimize the square of the difference between theoretical and measured positions are calculated. Further assignments are made, followed by refinement. This process is continued until all observed components are assigned; then, all the hyperfine constants (upper and lower) are fit simultaneously. Typically, the fits are within ± 12 MHz. In calculating the ground-state hyperfine constants, a number of transitions are simultaneously fit.

 0030-3941/79/020230-03$00.50